The Santa Cruz Basin Submarine Landslide Complex, Southern California: Repeated Failure Of Uplifted Basin Sediment

Chapter · June 2018

DOI: 10.2110/sepmsp.110.05

5 authors, including:

Daniel S. Brothers
United States Geological Survey
80 PUBLICATIONS **539** CITATIONS

SEE PROFILE

Katherine Leigh Maier
National Institute of Water and Atmospheric Research
47 PUBLICATIONS **382** CITATIONS

SEE PROFILE

Jared W. Kluesner
United States Geological Survey
49 PUBLICATIONS **227** CITATIONS

SEE PROFILE

J. E. Conrad
United States Geological Survey
44 PUBLICATIONS **390** CITATIONS

SEE PROFILE

THE SANTA CRUZ BASIN SUBMARINE LANDSLIDE COMPLEX, SOUTHERN CALIFORNIA: REPEATED FAILURE OF UPLIFTED BASIN SEDIMENT

DANIEL S. BROTHERS, KATHERINE L. MAIER, JARED W. KLUESNER, JAMES E. CONRAD
Pacific Coastal and Marine Science Center, US Geologic Survey,
2885 Mission Street, Santa Cruz, California 95060 USA
e-mail: dbrothers@usgs.gov

AND

JASON D. CHAYTOR
Woods Hole Coastal and Marine Science Center, US Geologic Survey,
384 Woods Hole Road, Woods Hole, Massachusetts 02540 USA

Abstract: The Santa Cruz Basin (SCB) is one of several fault-bounded basins within the California Continental Borderland that has drawn interest over the years for its role in the tectonic evolution of the region, but also because it contains a record of a variety of modes of sedimentary mass transport (i.e., open slope vs. canyon-confined systems). Here, we present a suite of new high-resolution marine geophysical data that demonstrate the extent and significance of the SCB submarine landslide complex in terms of late Miocene to present basin evolution and regional geohazard assessment. The new data reveal that submarine landslides cover an area of ~160 km^2 along the eastern flank of the Santa Rosa–Cortes Ridge and have emplaced a minimum of 9 to 16 km^3 of mass transport deposits along the floor of the SCB during the Quaternary. The failures occur along an onlapping wedge of Pliocene sediment that was uplifted and tilted during the later stages of basin development. The uplifted and steepened Pliocene strata were preconditioned for failure so that parts of the section failed episodically throughout the Quaternary—most likely during large earthquakes. Once failed, the material initially translated as a block glide along a defined failure surface. As transport continued several kilometers across a steep section of the lower slope, the material separated into distinctive proximal and distal components. The failed masses mobilized into debris flows that show evidence for dynamic separation into less and more mobile components that disturbed and eroded underlying stratigraphy in areas most proximal to the source area. The most highly mobilized components and those with the lowest viscosity and yield strength produced flows that blanket the underlying stratigraphy along the distal reaches of deposition. The estimated volumes of individual landslides within the complex (0.1–2.6 km^3), the runout distance measured from the headwalls (>20 km), and evidence for relatively high velocity during initial mobilization all suggest that slides in the SCB may have been tsunamigenic. Because many slopes in the California Continental Borderland are either sediment starved or have experienced sediment bypass during the Quaternary, we propose that uplift and rotation of Pliocene deposits are important preconditioning factors for slope failure that need to be systematically evaluated as potential tsunami initiators.

Key words: submarine landslide, mass transport deposit, sediment flow, tsunami hazards, multichannel seismic

INTRODUCTION

The southern California Continental Borderland ("Borderland") is characterized by a complex Neogene and Quaternary geologic history marked by a series of shifts in the style and rate of tectonic deformation along the margin of western North America (Moore 1969, Vedder 1987, Legg 1991, Crouch and Suppe 1993, Nicholson et al. 1994, Atwater and Stock 1998, Bohannon and Geist 1998, ten Brink et al. 2000, Legg et al. 2007). As subduction of the Farallon plate ceased during the early–middle Miocene, and the Pacific plate came into contact with the North American plate, a broad transform boundary began to form offshore southern California. Until the late Pliocene, when the majority of plate motion jumped ~200 km eastward to form the present-day San Andreas Fault System, most of the deformation was accommodated by strike-slip and oblique-slip faults in the Borderland, creating more than 20 fault-bounded basins and ridges that defined the physiographic setting of the Borderland throughout the most of the Pliocene and Quaternary (Shepard and Emery 1941, Moore 1969, Kamerling and Luyendyk 1985, Teng and Gorsline 1989, Legg 1991, Bohannon and Geist 1998, ten Brink et al. 2000, Chaytor et al. 2008). Furthermore, many of the basins in the Borderland are bounded by steep slopes with high relief that appear to be prone to seismically induced landsliding, which in turn may be capable of generating local tsunamis (Borrero et al. 2004, Fisher et al. 2005, Greene et al. 2006, Lee et al. 2009, Ryan et al. 2015). Several faults within the Borderland proper and along the boundary between the Borderland and the Transverse Ranges remain seismically active today (Pinter and Sorlien 1991; Lindvall and Rockwell 1995; Shaw and Suppe 1996; Astiz and Shearer 2000; Seeber and Sorlien 2000; Fisher et al. 2004; Legg et al. 2007; Chaytor et al. 2008; Lee et al. 2009; Ryan et al. 2009, 2012; Brothers et al. 2015; Legg et al. 2015; Conrad et al. 2018). Large earthquakes on any of these fault systems are potential triggers for landslide generation. Despite the recognition of these hazards, the types of high-quality bathymetric and subbottom data needed for comprehensive assessments have not become available until recently, and a significant portion of the Borderland seaward of the Channel Islands remains unexplored using systematic geophysical mapping techniques.

The Santa Cruz Basin (SCB) is a deep, northwest–southeast-trending trough located ~100 km to the west of Los Angeles and 5 km to the south of Santa Cruz Island (Fig. 1); it is physiographically isolated from the southern California mainland. Several marine geophysical and sediment sampling surveys were conducted in and around the SCB by Donn Gorsline and colleagues during the 1960s

From the Mountains to the Abyss: The California Borderland as an Archive of Southern California Geologic Evolution
DOI: http://dx.doi.org/10.2110/sepmsp.110.05
SEPM Special Publication No. 110, Copyright © 2017
SEPM (Society for Sedimentary Geology), ISBN 978-56576-354-8, eISBN 978-56576-355-5, p. 000–000.

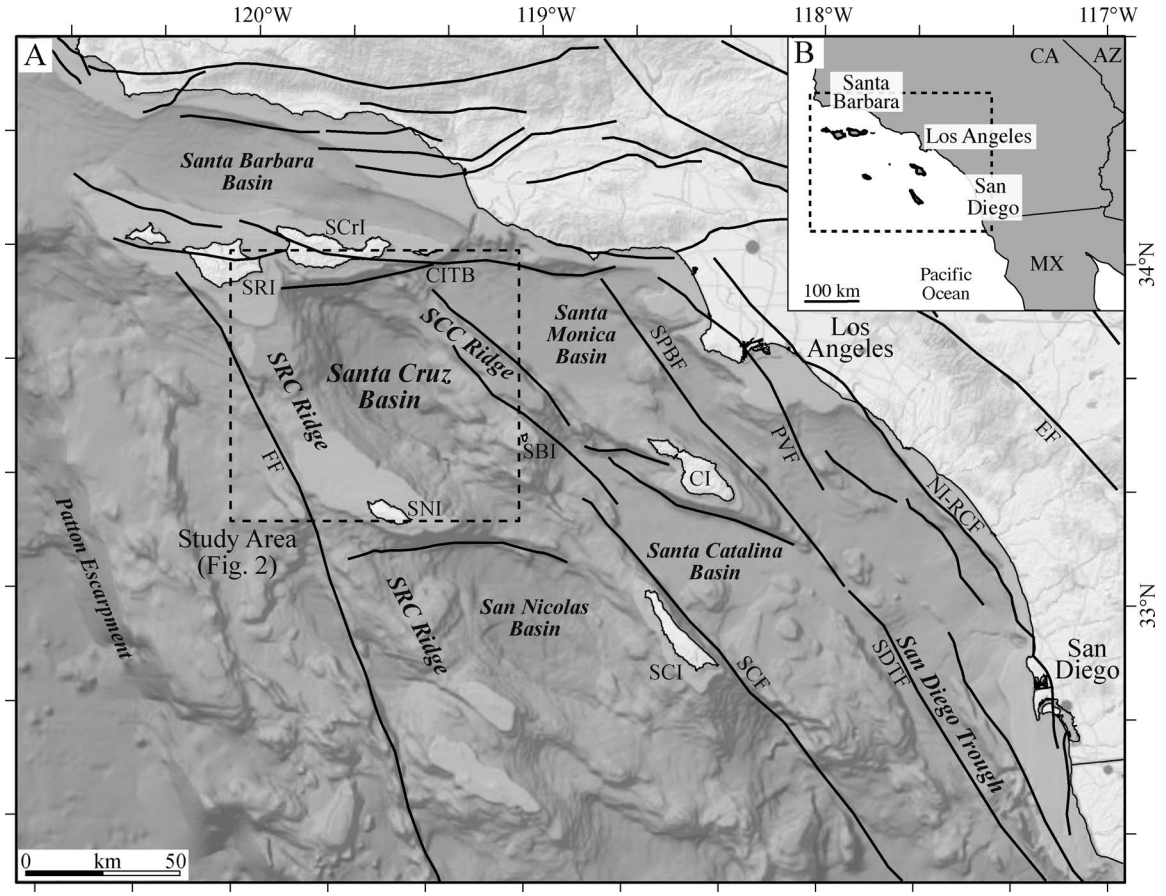

FIG. 1.—**A)** Shaded-relief bathymetry of the California Continental Borderland. Black lines are labeled fault zones: Ferrelo Fault (FF), San Clemente Fault (SCF), San Pedro Basin Fault (SPBF), San Diego Trough Fault (SDTF), Newport Inglewood–Rose Canyon Fault (NI-RCF), Elsinore Fault (EF), Channel Islands Thrust Belt (CITB). Geographic abbreviations: San Clemente Island (SCI), Santa Catalina Island (CI), Santa Barbara Island (SBI), San Nicolas Island (SNI), San Miguel Island (SMI), Santa Rosa Island (SRI), Santa Cruz Island (SCrI), Santa Rosa–Cortes (SRC) Ridge, and Santa Cruz–Catalina (SCC) Ridge. **B)** Regional location map.

and 1970s (Barnes 1970; Felsher 1971; Gorsline and Barnes 1972; Nardin et al. 1979a, 1979b; Field and Edwards 1980; Field and Richmond 1980; Schwalbach and Gorsline 1985; Teng and Gorsline 1989). These early studies recognized that mass wasting was an important deep-sea sedimentary process throughout the Borderland and documented the existence of a fairly large zone of seafloor within the SCB covered in submarine landslide debris. However, the limited resolution of bathymetric data and seismic reflection profiles at the time precluded an accurate assessment of the extent of landslide features in the SCB, their detailed morphological expressions, and their potential hazards. In this paper, we present a suite of new marine geophysical observations of a large submarine landslide complex along the western margin of the SCB and provide a preliminary assessment of the potential causes of slope failure. We also discuss the implications of these findings within the broader context of Borderland landslides as well as the potential for future landslides in the SCB to generate tsunamis that may impact the southern California coastline.

GEOLOGIC BACKGROUND

Since the late Miocene, fault-bounded ridges have enclosed the SCB on all sides, creating an effective sediment sink (Figs. 1, 2). The Santa Cruz–Catalina Ridge to the east of the SCB contains the East Santa Cruz Basin Fault System and the Santa Cruz–Catalina Ridge Fault System (Crouch and Suppe 1993, Bohannon and Geist 1998, ten Brink et al. 2000, Chaytor et al. 2008, Schindler 2010); undulating topography, localized ridges, gullies, sediment pockets, and knolls characterize this ridge. The northern wall of the SCB coincides with transpressional uplift along the Channel Islands Thrust Belt, which also marks the boundary between the Borderland and the Transverse Ranges Province to the north (Pinter and Sorlien 1991, Shaw and Suppe 1996, Seeber and Sorlien 2000, Chaytor et al. 2008). The northern wall is steep and rugged and cut by the Santa Cruz submarine canyon and several smaller canyon and gully networks (Figs. 2, 3; Barnes 1970, Felsher 1971, Chaytor et al. 2008). The Santa Rosa–Cortes Ridge (SRCR) to the west of the SCB is the northern extension of a broad northwest-trending anticlinorium (Moore 1969, Field and Richmond 1980, Vedder 1987), bounded on its western flank by the Ferrelo Fault (Junger 1976, Vedder 1987, Legg et al. 2015). The ridge top sits mostly between water depths of 100 and 200 m, but it increases in depth to over 350 m at a bathymetric saddle about halfway between Santa Rosa and San Nicolas islands. Overall, the ridge has up to 1800 m of relief relative to the floor of the SCB (Fig. 2). The broad eastern flank of the SRCR spans over 1200 km^2 and displays little to

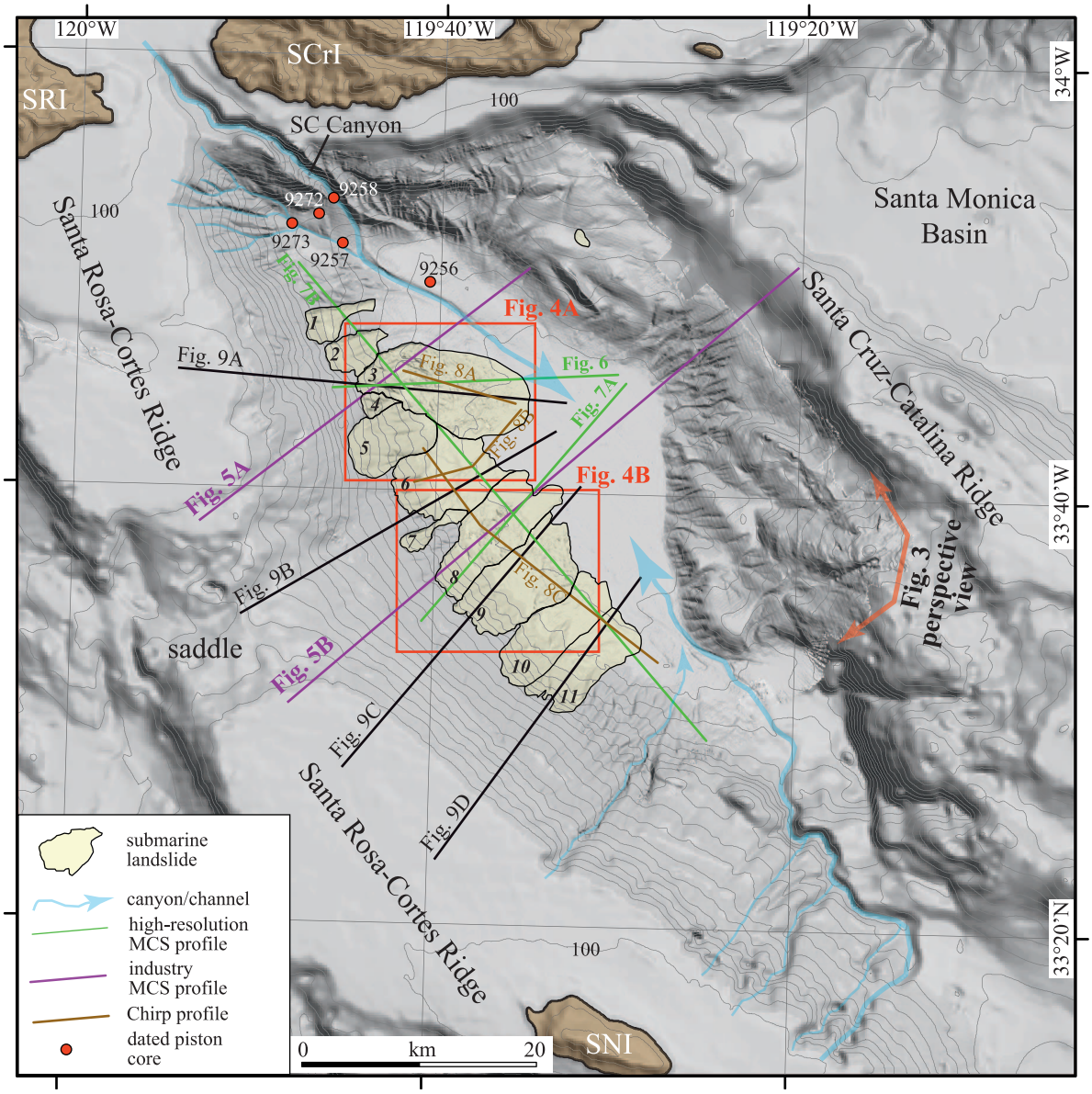

FIG. 2.—Shaded-relief bathymetry of the Santa Cruz Basin and surrounding terrain; bathymetric contours depict 100 m intervals. Submarine landslides identified in high-resolution bathymetry data are outlined and shaded in yellow (see Figs. 3, 4). Seismic reflection profiles and bathymetric profiles shown in subsequent figures are labeled on the map. Canyon/channel pathways, in blue, show spatial relationship between the dominant modes of Quaternary sediment delivery (i.e., mass wasting from the ridge flank vs. sediment flows sourced from submarine canyons; Felsher 1971). Red circles are locations of piston cores from Felsher (1971) that provided radiocarbon dates and estimates for late Pleistocene to present sedimentation rates in the northern basin. Abbreviations: Santa Rosa Island (SRI), Santa Cruz Island (SCrI), San Nicolas Island (SNI), Santa Cruz (SC) canyon.

no significant canyonization or localized Quaternary faulting, giving it a smooth appearance.

The following paragraph from Teng and Gorsline (1989 p. 30) provides a fundamental description of Borderland basin development and can be used to understand the first-order evolution of the SCB:

> Because the borderland has undergone intense tectonism throughout Neogene time, most of the areas have experienced more than one diastrophic upheaval. The distribution of pre-late Miocene sediment bears no distinct relationship to the present configuration of any of the basins, and only the post-late Miocene sediments are affected by the geometry of the present-day basins. Hence, the contemporary borderland basins probably did not begin to take shape until late Miocene. The upper Miocene sequences are composed of diatomaceous shales comparable to the Monterey shale. . . and commonly form draped sequences that cover bathymetric irregularities. Although some of the Miocene sediments thicken toward the centers of the

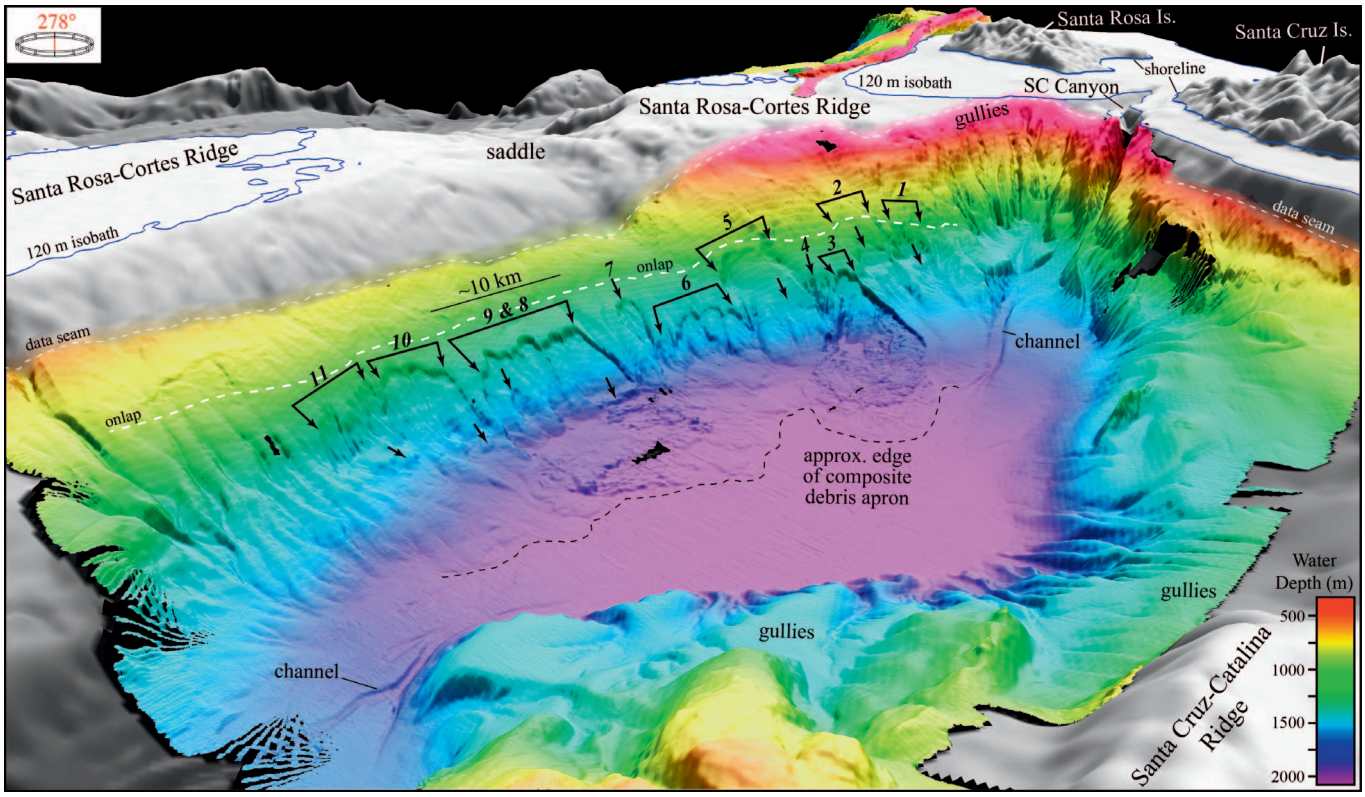

FIG. 3.—Three-dimensional perspective view looking west (278°) at the eastern flank of the Santa Rosa–Cortes Ridge. Distinctive headwall scarps are identified and numbered based on the extent and angularity of the scarp. The dashed black line marks the approximate edge of the debris aprons having positive relief, although subbottom profiles show the distal slide deposits extending across the entire basin floor; dashed white line on the slope is the approximate location of Pliocene onlap (see Figs. 5–7). Colored multibeam bathymetry data were acquired by NOAA ship *Okeanos Explorer* in 2011; grayscale bathymetry is from the 90 m Coastal Relief Model (National Geophysical Data Center 2013).

basins, their distribution is not confined to the basins. Pliocene–Quaternary sediments occur as flat-lying sequences that fill topographic lows of the basins and were deposited by processes controlled by the basin morphology.

The SRCR is an anticlinal structure that developed almost continuously during the Miocene and Pliocene, with some minor deformation occurring during the Pleistocene (Field and Richmond 1980, Vedder and Howell 1980). Almost all rock samples dredged and drilled from the ridge are of Miocene and Pliocene age (Field and Richmond 1980, Vedder 1987, Chaytor 2006). A broad erosional surface clearly marks the boundary between Miocene and Quaternary sediments on the ridge top. Repeated transgressions and regressions have truncated a series of complex fold and fault structures, producing a nearly flat surface (Junger 1976, Field and Richmond 1980). Because of the isolation of the SRCR from the mainland, there has always been very limited sediment supply to the ridge top. Fluctuations in sea level, particularly during transgression, eroded the ridge top and transported sediment into the bathymetric lows and over the edges. On the upper flanks of the ridge, some Pleistocene terrace deposits are preserved that are up to 20 m thick (Field and Richmond 1980), but most of the ridge top is an area of nondeposition. Nardin et al. (1979a) suggested that sediment transport down the flanks of the ridge is presently active and accounts for thin sand layers found in the surficial layer of predominantly hemipelagic sediments.

The vast majority of sediment enters SCB through canyon–channel systems at the northern and southern ends of the basin and via mass wasting along the eastern flank of the SRCR. The Santa Cruz canyon, an active canyon system that cuts the northern slope, has been the focus of several studies in the SCB (Barnes 1970, Felsher 1971, Schwalbach et al. 1996) and has been a major sediment conduit to the SCB throughout the Quaternary. The canyon captures terrigenous sediment from the adjacent Channel Islands platform that is transported downslope to an ~30 km^2 distributary fan and channel system on the basin floor (Barnes 1970, Felsher 1971, Schwalbach et al. 1996). Early studies noted that eastward meanders in the trunk channel appear to be deflected around slump features originating from the east-facing flank of the SRCR (e.g., Felsher 1971). Other canyon-valley systems are observed on the slopes of the southern end of SCB, at least three of which are morphologically significant canyon–channel systems that capture sediment from the shelves surrounding San Nicolas and Santa Barbara islands and debouch onto the basin floor (Barnes 1970, Felsher 1971; Fig. 2).

Deposits from submarine landslides (aka "slides") were first recognized in the SCB by Barnes (1970) and noted as potential geological hazards by Greene et al. (1975) and Nardin et al. (1979a). Nardin et al. (1979a) suggested the slumps, scarps, and deposits in the northwestern part of the basin were part of a larger landslide complex

and provided a detailed description of a major slide along the northwestern portion of the slope that will be discussed in detail in this paper (i.e., slide 3). Based on sedimentation rates from Barnes (1970) and Felsher (1971), the upper lens of the northwestern landslide complex was estimated to be late Pleistocene to early Holocene in age, and box cores from this same region suggested that smaller landslides may have continued into the Holocene (Nardin et al. 1979a). Nardin et al. (1979a) also described the slide deposits along the lower slope as a mechanical continuum of decreasing viscosity and strength moving from proximal to distal zones of deposition (e.g., block slides and slumps mobilizing into progressively more fluid debris flows and perhaps turbidity currents).

Hemipelagic sedimentation is providing the bulk of the material now being deposited in the SCB. However, the age and rate of deposition differ greatly between the basin floor, where meters of Holocene deposits (likely including debris flows and turbidites) have accumulated, and the adjacent slopes and ridges, which have thinner sediment cover and contain outcropping Miocene deposits (Barnes 1970, Felsher 1971, Nardin et al. 1979a). Using sediment core samples and 3.5 kHz subbottom profiles, Nardin et al. (1979a) distinguished different types of mass transport deposits: slides (block movement along a failure surface), flows resulting from remolding and mobilization of deforming blocks, and landslide-derived turbidites. Significant transport into the basin from the surrounding ridges is indicated by shallow-water foraminifera found deposited on the basin floor (Schwalbach et al. 1996). Core samples of the upper 2 m of sediment contain layered deposits with features indicative of turbidites (e.g., Bouma T_b laminated carbonate-rich sand beds and loaded bases of sand beds; Bouma et al. 1962) and deformed sediments with sharp bases suggestive of mass transport deposits that eroded at their bases as they moved onto the basin floor (Barnes 1970, Nardin et al. 1979a). Total undecompacted sedimentation rates are on the order of 0.2–0.8 mm/yr throughout the basin for the late Pleistocene–early Holocene (from Nardin et al. 1979a, based on sediment accumulation estimates in Barnes 1970). Biostratigraphic dating of foraminifera indicated that the base of an ~12,000-year-old layer is at 6+ m below the basin floor (Gorsline and Barnes 1972). Beyond results from these early studies, the late Pleistocene to present sedimentation history in the SCB remains poorly constrained and is expected to exhibit a significant amount of spatial variability depending on the proximity to canyons, channels, and sources of mass transport deposits.

DATA AND METHODS

A suite of recently acquired, high-resolution marine geophysical data was used to characterize the seabed morphology, map the distribution of submarine slides, and examine the shallow substrate architecture of the SCB and adjacent basin margins (Fig. 2). Raw multibeam bathymetry data from numerous surveys across the study region were obtained from the National Oceanic and Atmospheric Administration (NOAA) National Centers for Environmental Information repository (NCEI; http://www.ngdc.noaa.gov/mgg/bathymetry/relief.html), edited and combined into a mosaic grid at 50 m cell spacing, following Dartnell et al. (2015). The principal data set for this study came from the NOAA ship *Okeanos Explorer* in April 2011 (https://www.ngdc.noaa.gov/ships/okeanos_explorer/EX1101_mb.html), which acquired multibeam bathymetry, acoustic backscatter, and water-column backscatter data along the east flank of the SRCR, the SCB, and the west flank of the Santa Cruz–Catalina Ridge using a hull-mounted Konsberg EM-302 (30 kHz) multibeam echosounder. Finalized raster surfaces were gridded to 30 m cell spacing for multibeam data and 10 m for backscatter mosaics. These data were combined with the southern California Coastal Relief Model (National Geophysical Data Center 2013), a regional-scale, 90-m-grid-resolution data set that represents an integration of publicly available single-beam and multibeam coverage (Figs. 2, 3). Due to the blending of data sets of highly variable resolutions, the Coastal Relief Model is most useful for first-order morphological analyses of the areas that do not contain continuous multibeam data coverage. Morphometrics of particular seabed features, such as headwall and sidewall scarps, slide evacuation zones, debris aprons, and slope profiles, were extracted from bathymetric data using ESRI ArcGIS.

In November 2014, the US Geological Survey (USGS) led a high-resolution multichannel seismic (MCS) survey in the SCB and nearby Santa Catalina Basin aboard the R/V *Robert Gordon Sproul*. Data were acquired using a 48 channel (6.25 m group spacing) Geometrics GeoEel digital hydrophone streamer, a 700 J Applied Acoustics power supply, and a Services and Instruments of Geophysique minisparker sound source. A relatively sparse grid totaling ~400 line-km was acquired in the SCB, with track lines arranged to target submarine landslides observed in the multibeam bathymetry data. The following processing steps were applied to each line: 60 to 900 Hz zero-phase band-pass filter, trace edit, fk-filter, common depth point sort, normal moveout correction (1500 m/s constant velocity), stack, and constant velocity phase migration. More rigorous processing, such as velocity analysis, dip moveout, and phase migration, was applied to a subset of profiles that were used for detailed geological interpretation (Fig. 2; Sliter et al. 2017). The minisparker acoustic source provided a relatively broad frequency band between ~100 and 700 Hz, with 5 to 10 m vertical resolution and up to 500 ms (~400 m) of subbottom penetration. Although Knudsen Chirp profiles were acquired simultaneously with the sparker profiles, data quality was poor, but some profiles did reveal important characteristics of the shallowmost 10 to 20 m of sediment. Additional Chirp profiles in the study area were obtained from NCEI geophysical data archives. Travel time to depth conversions in high-resolution profiles assumed a 1500 m/s velocity. Interpretation of seismic stratigraphy and analyses of the relationships between substrate architecture and seabed morphology were conducted using IHS Kingdom Suite.

To better understand the linkages between the shallow, Quaternary-aged stratigraphy and the underlying, older Pliocene–Miocene basin framework, thousands of line-kilometers of regional-scale, 1970s and 1980s vintage MCS reflection profiles were obtained from the USGS National Archive of Marine Seismic Surveys (NAMSS; https://walrus.wr.usgs.gov/NAMSS/) and loaded into Kingdom Suite. Select profiles from Western Geco surveys are presented in this study (lines WC82-116 and WC82-100) and span not only the SCB, but also the surrounding ridges (Fig. 2). These legacy data provide 30 to 50 m vertical resolution and up to 6 seconds of penetration (two-way travel time). Navigational offsets within the legacy profiles, arising from the limited positioning capabilities at the time of acquisition, were corrected by shifting profiles to align with correlative seafloor features in the high-resolution multibeam bathymetry data.

We identified variations in stratal geometry, reflectivity, and character that allowed us to infer changes in the depositional processes over time (i.e., seismic facies analysis; Mitchum et al. 1977, Teng and Gorsline 1989). We also assigned key chronostratigraphic horizons identified in previous studies based on sediment coring, seabed dredge sampling, and well logs (e.g., Barnes 1970, Felsher 1971, Nardin et al. 1979a, Field and Richmond 1980, Schindler 2010). However, many of the correlations are tentative due to the limited navigational accuracy of samples acquired in the 1960s and 1970s, but also due to the inherent limitations in correlation of two-dimensional (2-D) seismic horizons across a broad region. Furthermore, limited numbers of radiocarbon samples from piston cores acquired in the 1960s provide some age control for late Pleistocene and Holocene sedimentary deposits in the northwestern margin of the SCB (Fig. 2). However, age estimates for major slides presented herein are based on relative dating and crosscutting

relationships; absolute dating of the slides is not possible with the available data.

RESULTS

Morphological Description

High-resolution shaded-relief bathymetry reveals complex and diverse seabed morphology within the SCB and along the surrounding ridge flanks. As noted by previous workers, steep, rugged slopes, gully networks, and incision by the Santa Cruz canyon dominate the northern slope of the basin (Figs. 2, 3). A well-defined canyon thalweg can be traced from the shelf between Santa Rosa and Santa Cruz islands to the base of the slope, where it transitions into a channel/fan system that extends basinward for more than 20 km (Figs. 2, 3). Other significant gullies and canyons emanate from the edge of the SRCR and continue down the slope and onto the southern portion of the basin floor. Several networks of gullies are distributed across the undulating western flank of Santa Cruz–Catalina Ridge and debouche into SCB. As noted by Chaytor et al. (2008), the eastern margin of the SCB, along the flank of the Santa Cruz–Catalina Ridge, displays substantial variation in steepness and directionality of local slopes.

The morphology of the western margin of the basin, also the east face of SRCR, is markedly different from the other margins in two ways. First, the aspect calculations for a smoothed, down-sampled (200 m grid) version of the Coastal Relief Model reveal that >90% of the slope is facing between 45° and 90°, and the mean downslope-oriented seabed gradient in 200 to 1600 m water depths is consistently between 6° and 9°. Second, the middle to lower slope (1000–1400 m water depth) is covered by a series of arcuate headwall and sidewall scarps ranging in length from 1 to 12 km. The angularity/steepness of the scarps is highly variable, with some displaying sharp rollover from the slope to the scarp face, whereas others are rounded and show subtle gullies or rills incised into the scarp face (Figs. 3, 4). In some cases, additional scarps are observed below the headwall. The slope above the scarps is relatively smooth, but it does display a hummocky character in the downslope direction, as noted by previous workers (Felsher 1971, Field and Richmond 1980). Along the basin floor below each of the scarps, there are broad debris aprons of positive relief that are characterized by lobate zones of blocky, hummocky, and stepped morphology. Some of the aprons are laterally and frontally confined and display toe scarps that progressively step down and grade into the flat basin floor. The scarps and the debris aprons observed in the multibeam data display characteristic morphologies associated with submarine slides (Hampton et al. 1996, Mulder and Cochonat 1996). Slope failures evacuated sediment from the region surrounded by the scarps and then transported and emplaced the failed masses at the base of the slope. Although previous studies also observed mass wasting features along the flank of the SRCR, the morphological character and spatial extent of the scarps and debris aprons were previously unresolved. Slope failure, slide generation, and mass transport deposition have overprinted approximately 380 km^2 of seafloor along the base of the SRCR (Figs. 2, 3).

Morphometric parameters for individual slides were extracted from the high-resolution multibeam data using geographic information system analysis and are summarized in Table 1. Slide area and volume are approximate measures of the evacuation zone, which is defined as the void space bounded by headwall/sidewall scarps and the upslope limit of the debris apron. Because the headwall and sidewall scarps are relatively well defined in the bathymetry data, and relatively intact patches of the slope between evacuation zones provide an idea of the slope morphology prior to failure, we propose that our volume estimates are accurate to within <10%. At least 11 individual slide scars can be distinguished in the multibeam data based on the continuity and character of their headwall and sidewall scarps (Figs. 2, 3). For example, three of the slides (slides 3, 8, and 9; Fig. 4) display evacuation zones bounded by steep and angular scarps, morphological evidence for downslope transport of failed masses, and emplacement of blocky, rugged debris lobes on the basin floor. Scarps bounding slides 5, 6, 7, and 10 are slightly rounded and less steep, and their evacuation zones show evidence for gullying and channelization. The depositional lobes associated with these slides have lower rugosity than those of slides 3, 8, and 9. Finally, scarps bounding slides 1, 2, 4, and 11 are subtle and highly rounded and show evidence for degradation and erosion associated with gully formation. The evacuation zones of slides 1, 2, 4, and 11 appear to be overprinted by subsequent erosion and deposition, and no identifiable debris apron can be confidently linked to a particular evacuation site based on seafloor morphology alone, suggesting the deposits are currently buried or reworked by younger slides. We also observed crosscutting relationships between adjacent slide scarps and deposits that can be used to examine relative ages. For example, the headwall and sidewall scarps bounding slide 3 appear to cut into the seafloor below slides 2, 4, and 5, and the debris lobe linked to slide 3 appears to be deposited on top of debris from slides 5 and 6 (Fig. 4A). Slides 8 and 9 share the same headwall and have indistinguishable debris lobes, but they appear to be separated by a sidewall scarp within the evacuation zone (Fig. 4B). Both slides have similar character as slide 3 and appear to have cut into previous slide surfaces and deposited debris on top of material derived from adjacent slides. Relative ages in Table 1 were assigned based on crosscutting relationships, the thickness of hemipelagic drape, and the angularity/rugosity of the slide scarps and debris lobes. Detailed descriptions of these parameters are provided in subsequent sections.

Substrate Architecture

Deep-penetration seismic reflection profiles across the study region show a series of eastward-dipping, parallel and subparallel reflectors that can be traced continuously from the SRCR to the western flank of the Santa Cruz–Catalina Ridge (Fig. 5). The approximate locations of allostratigraphic units identified in previous studies (Teng and Gorsline 1989, Schindler 2010) are shown on two type sections in Figure 5. A high-amplitude reflector with "ropey" character corresponds to the basement–sediment interface, and a thick wedge of Cretaceous to Paleogene sedimentary sequences overlies the basement rock (Teng and Gorsline 1989). Internal reflectors appear to mimic the basement topography, but several of the upper packages are truncated beneath the Santa Cruz Basin by a Lower Miocene unconformity surface, which can be traced throughout the western SCB. The overlying Miocene package defines the substrate for most of the SRCR and upper slope of the ridge flank. Internal reflectors are mostly parallel and continuous, but they also show varying amounts of truncation at the seafloor. Faulting and folding are observed in Miocene and older strata along the SRCR and in Pliocene and older strata in the SCB (Fig. 5; Field and Richmond 1980, Schindler 2010). The total post-Miocene basin fill appears to be ~500 m thick in the deep-penetration MCS profiles (Schindler 2010).

The Pliocene–Quaternary section is mostly confined to the floor of the SCB and is imaged in substantial detail in the high-resolution MCS profiles (Figs. 6, 7). Type sections across slides 3 and 8, the two most geomorphically pronounced failures identified in the SCB (e.g., Fig. 4), can be seen in Figures 6 and 7A. In general, Pliocene reflectors display eastward divergence, thickening, and decreasing dip up section (Fig. 5), whereas Quaternary reflectors are more flat-lying and appear to onlap the basin margins. Two important stratigraphic features are observed in the Pliocene–Quaternary section along the flank of the SRCR: (1) A package of basinward-dipping, early Pliocene strata onlaps the middle slope of the SRCR at a fairly consistent depth along the length of the slope (between 800 and 1050

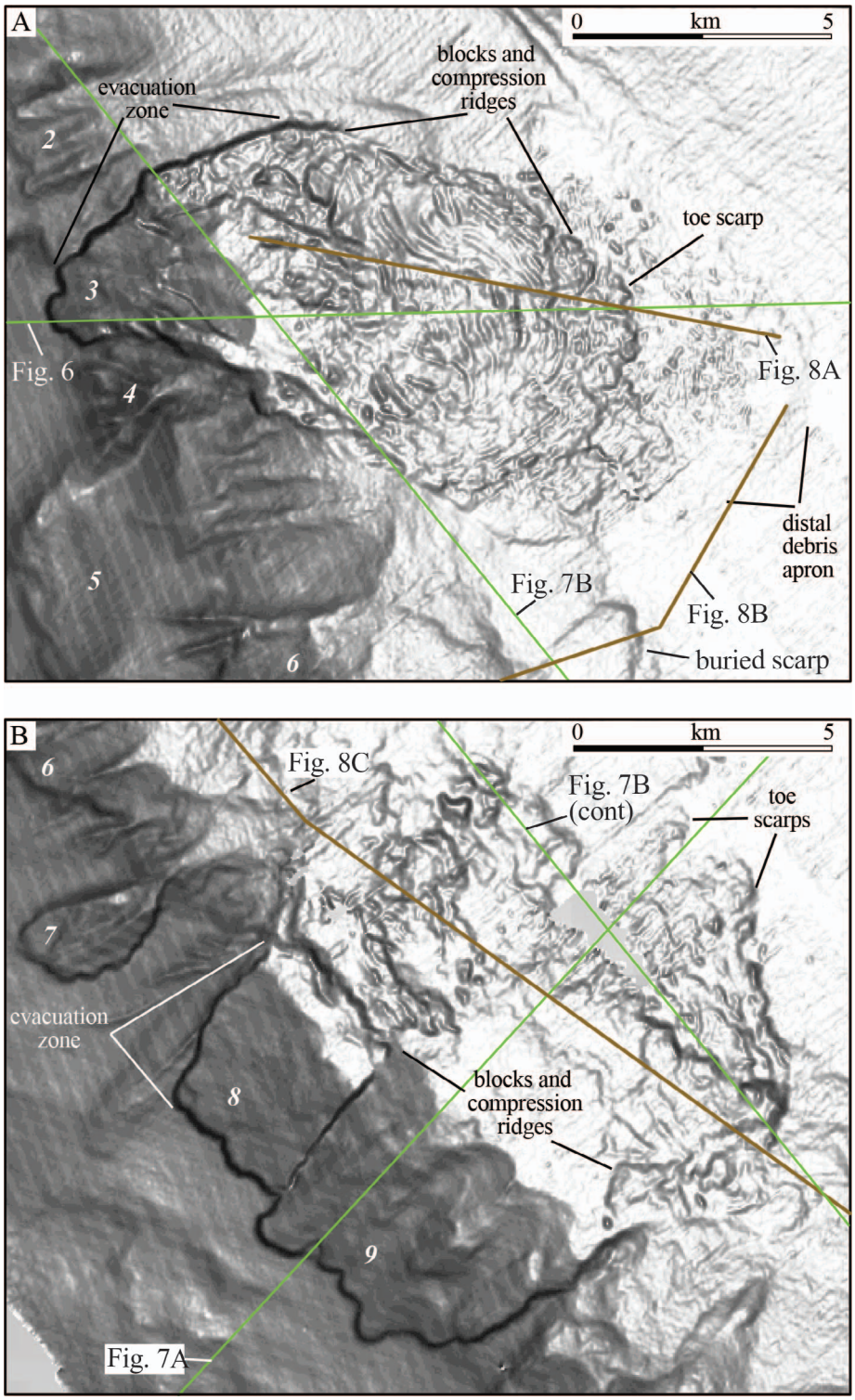

FIG. 4.—Enlarged views of slide morphology along the eastern flank of the Santa Rosa–Cortes Ridge. See Figure 2 for locations. Shaded-relief data are 20 m resolution; green lines are multichannel seismic profiles; brown lines are subbottom Chirp profiles.

TABLE 1.—Summary of Santa Cruz Basin slide metrics and inferred relative age estimates based on morphological expression and thickness of postslide sediment drape; "relative age" numbers range from 1 (youngest) to 8 (oldest).

Slide number	Minimum area of evacuation zone (km^2)	Identifiable mass transport deposit (MTD)?	Minimum runout (km)	Volume (km^3)	Headwall water depth (m)	Headwall height (m)	Relative age (1 = young, 8 = old)	Description/comments
1	9	No	?	0.5–0.9	1050–1150	80 ± 20	7	Nested scarps; rounded, degraded. gullied headwall; no identifiable MTD
2	12	No	?	0.5–0.7	900–1100	50 ± 10	7	Nested scarps; rounded, degraded, scalloped headwall; no identifiable MTD
3	21	Yes	20	1.7–2.5	1275–1600	100 ± 20	1	Continuous and angular headwall and sidewall; clear MTD; no drape
4	5	No	?	0.1–0.4	1275–1400	50 ± 30	6	Degraded, gullied headwall; no identifiable MTD
5	21	No		1.3–2.1	1050–1200	80 ± 20	5	Nested scarps; rounded, degraded, scalloped headwall; gullies below scarp; MTD buried beneath slide 3
6	15	Yes	9	0.6–0.9	1400–1550	50 ± 10	4	Nested scarps along and across slope; slightly rounded, degraded, scalloped headwalls; gullies below scarps; MTD buried, above slide 5
7	4	Yes	9	0.2–0.3	1250–1350	60 ± 10	4	Continuous and angular headwall and sidewall; narrow failure zone; gullying below headwall; no identifiable MTD
8	13	Yes	20	1.0–2.6	1275–1350	100 ± 20	2	Nested scarps along and across slope; continuous and angular headwall; clear MTD; sidewall scarp separating slides 8 and 9, but continuous headwall; slightly buried composite MTD
9	22	Yes	20	1.8–2.6	1275–1350	100 ± 20	2	
10	20	Yes	11	0.8–2.0	1150–1300	70 ± 30	4	Nested scarps along and across slope; slightly rounded, degraded, scalloped headwalls; gullies below scarps; MTD buried with similar stratigraphic position as slide 6
11	21	Yes	10	1.0–2.3	1200–1350	80 ± 30	8	Nested scarps; heavily gullied, degraded, scalloped headwall; buried MTD with similar stratigraphic position as slide 5
Sum total/average	163/14.8	–	13.8	9.5–16.3/1.2	1263	75	–	

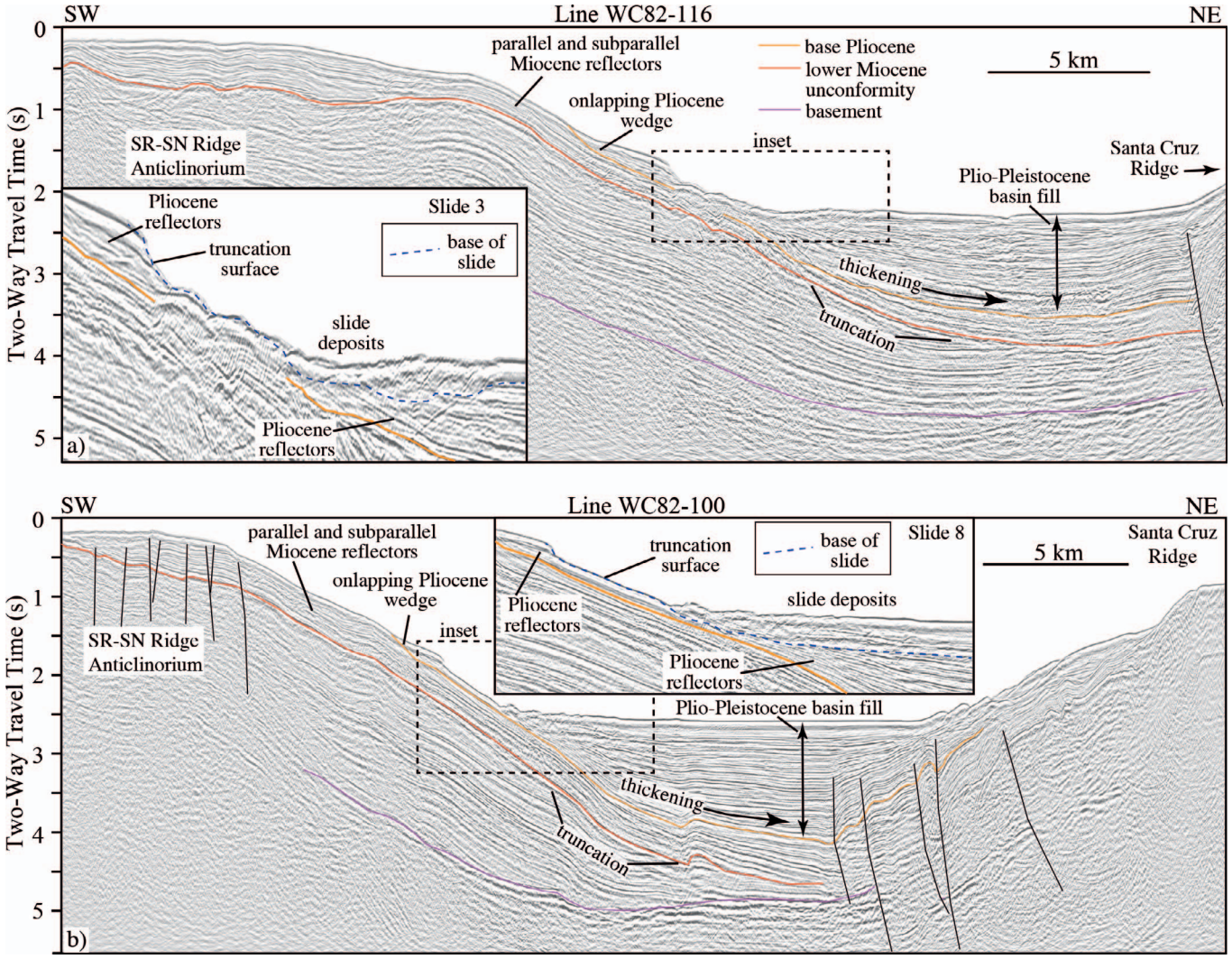

FIG. 5.—Deep-penetration seismic reflection profiles highlighting the basin architecture and key stratigraphic units. Horizon mapping is adapted from Teng and Gorsline (1989) and Schindler (2010). Data were obtained from USGS NAMSS (https://walrus.wr.usgs.gov/NAMSS/). See Figure 2 for profile locations. Vertical black lines represent faults.

m; see "onlap" in Figs. 3, 5–7); and (2) the onlapping package is truncated by failure scarps along the length of the SRCR, but the intact reflectors on the slope above the headwalls are inferred to be correlative with truncated reflectors that are buried at the base of slope beneath slide deposits (Fig. 5, inset; Figs. 6, 7). The basal failure surfaces for each of the slides appear to correspond to steeply dipping stratigraphic contacts within the early Pliocene section. Along the basin floor, reflectors imaged in the uppermost 100 m are essentially flat lying and continuous except in areas that have been disrupted by slide deposits. We observed no evidence for local fault/fold-related deformation that may be influencing the spatial distribution of headwall scarps. The only definitive evidence for Quaternary fault/fold activity is along the eastern margin of the SCB (Fig. 5), as described previously by Chaytor et al. (2008) and Schindler (2010).

Slide deposits display considerable variation in thickness and internal character depending on the distance from their respective evacuation zones. Deposits most proximal to the lower slope are relatively thick (100–250 m) masses of intensely deformed and/or chaotic reflectors resting above a basal contact that overlies sections of heavily deformed and truncated strata. The deposits show abrupt changes in thickness and degree of disturbance in the underlying strata in places directly below compression ridges and toe scarps (e.g., Figs. 6, inset; Fig. 7A, inset). For slides 3, 8, and 9, an acoustically transparent layer of nearly uniform thickness (10–20 m) extends from the toe scarp across the width of the basin ("distal deposit" in Figs. 6, 7A). The entire slide 3 deposit appears to be exposed at the seafloor, but the fine-scale crosscutting relationships (uppermost few meters of the substrate) with deposits from the Santa Cruz channel/fan system are unresolved. In contrast, the basinward extension of slide 8 is covered by 10 to 60 m of parallel-bedded reflectors that appear to onlap positive relief of the proximal deposit. The estimated runout distance for individual slides (e.g., 3, 8, and 9) exceeds 20 km. Several older slide deposits are buried along the base of the slope and above a dipping horizon inferred to be the approximate position of the Pliocene–Pleistocene boundary (Figs. 6, 7). Figure 7B illustrates the superpositioning of slide deposits along the length of the slope. Buried slide deposits were matched with distinct

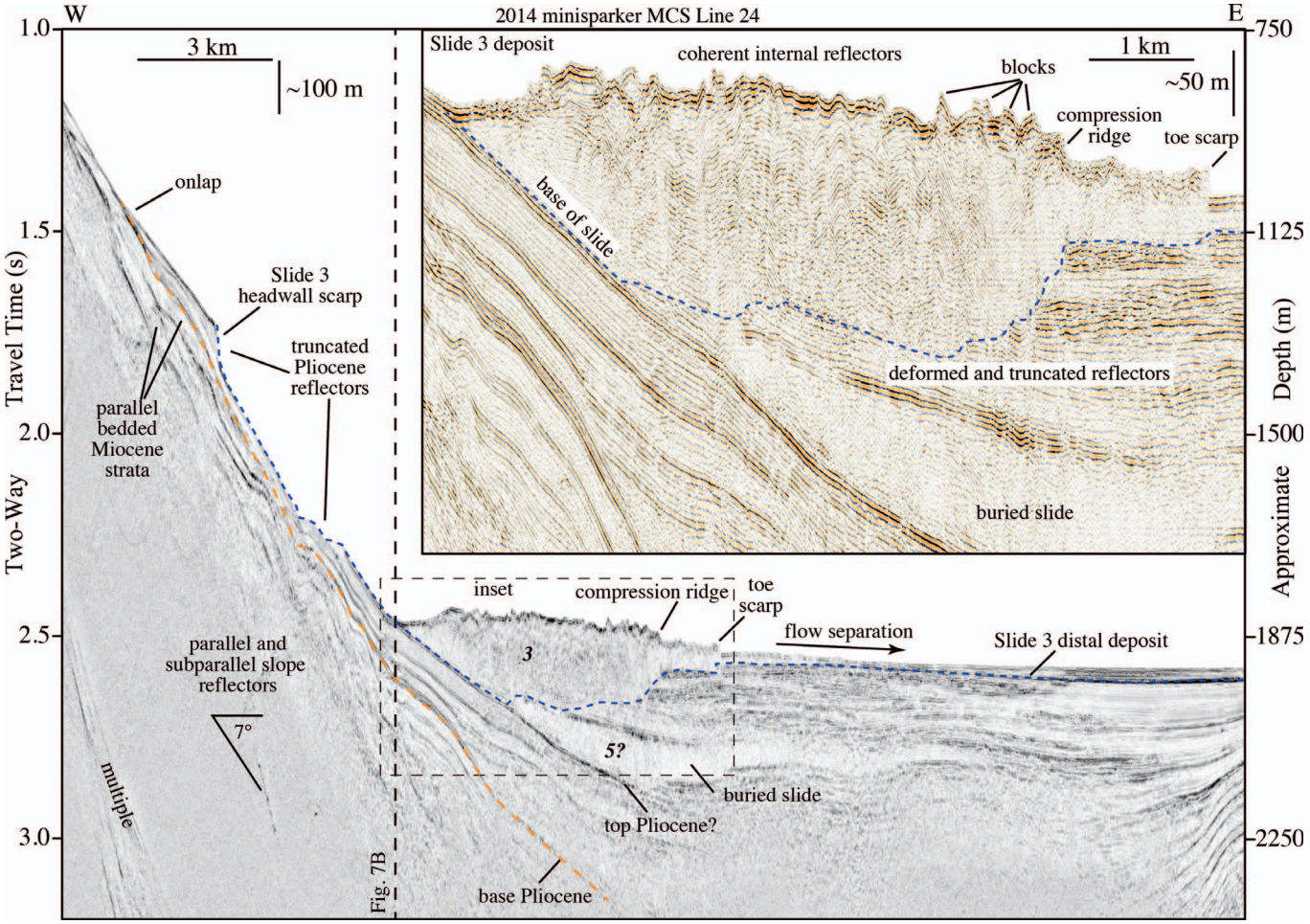

FIG. 6.—High-resolution multichannel sparker profile spanning the evacuation and deposition zones of slide 3. The grayscale image is the envelope attribute (positive amplitudes only; no phase or polarity information). Note the along-profile variation in seafloor morphology, thickness, and internal character of the slide deposit. Inset shows an enlarged section of the proximal slide deposits, highlighting evidence for highly deformed internal reflectors and correspondence between deposit thickness and morphological features on the seabed (i.e., compression ridges and toe scarps), suggestive of flow separation. The color image is the full-waveform amplitude data. See Figure 2 for profile location and Figure 5 for key to colored horizons.

headwall scarps by visually aligning the spatial extent of evacuation zones to that of the deposits. Although the deposits have widths similar to their associated evacuation zones, and the observed superposition can be used to estimate the relative ages of slides, several of the smaller and/or older slide deposits have either been reworked by subsequent slides into a composite, or they simply cannot be uniquely identified in the substrate (e.g., slides 1, 2, 4, and 7). Stacked, parallel and subparallel reflectors of variable amplitude characterize the seismic stratigraphy observed between slide deposits and along the eastern half of the SCB (Figs. 5–7).

Two downslope-oriented Chirp profiles cross slides 3, 5, and 6 (Fig. 8A, B), and an along-slope-oriented profile spanning the depositional zones of slides 5–11 (Fig. 8C) provides additional estimates for the relative ages of slides. The character of the uppermost 50 to 75 m of sediment is highly variable throughout the failure zone. Penetration into the proximal deposit of slide 3 is limited due to the rugged and blocky nature of the seafloor. We observed no evidence for sedimentary drape overlying the slide deposit (Fig. 8A). Penetration increases basinward, particularly beyond the toe scarp, where a faint basal reflector gradually increases in amplitude and coherency. As observed in the high-resolution MCS data (Fig. 6), the distal material emplaced above the basal reflector appears to be a continuous component of the larger slide deposit. In other words, there is no evidence for onlap or truncation that would suggest the proximal and distal regions of the slide were instead emplaced by separate events. In contrast, the evacuation zone for slide 6 (Fig. 8B) contains a relatively thick section (~60 m) of parallel reflectors that mantle an underlying basal horizon, which is interpreted to be the slide surface. Based on sedimentation rates documented in previous studies (e.g., Barnes 1970, Nardin et al. 1979a), the uppermost ~5- to 10-m-thick unit of draped material is likely to be Holocene; underlying draped strata are likely Pleistocene units. Draped layers on the basin floor appear to have been disrupted by slide 3, which overlies a series of reflectors that onlap a buried scarp within the evacuation zone of slide 6 (Fig. 8B). A stacked section of onlapping layers also has chaotic internal character suggesting these layers represent older slide deposits. Last, the along-slope profile (Fig. 8C) reveals substantial variation in the geometry and character of the slide zones. Slides 10 and 11 appear to

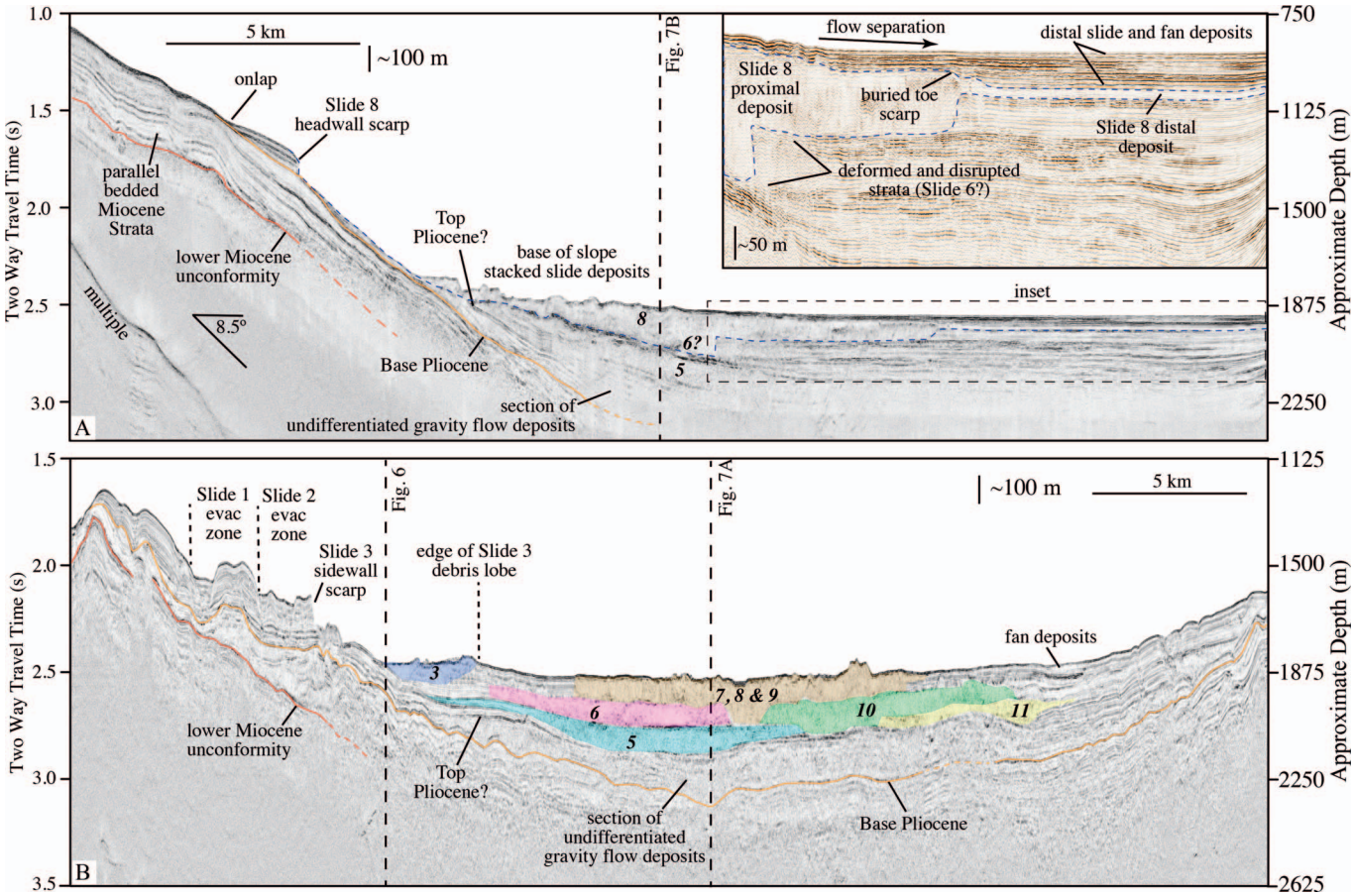

FIG. 7.—**A)** Across-slope high-resolution multichannel sparker profile across slide 8. The grayscale image is the envelope attribute (positive amplitudes only; no phase or polarity information). Inset is full-waveform amplitude data showing an enlarged section of the distal deposit. **B)** Along-slope profile crossing multiple slide deposits (colored layers labeled according to slide number). See Figure 2 for profile locations and Figure 5 for key to colored horizons.

be buried by ~40 m of parallel-bedded sediment. A thin layer of drape (0–10 m) has accumulated in local bathymetric lows between blocks of debris and along relative flat spots of slides 6–9.

Four bathymetric profiles were extracted from the Coastal Relief Model across the SRCR and into the SCB (Fig. 9). Comparisons between profile morphology and slide distribution reveal the following relationships: (1) There is no identifiable pattern that links slope failure to a particular morphological metric in the profiles (e.g., changes in gradient); (2) the slope contains relatively minor fluctuations in profile gradient, one of the most significant being a rapid decrease in gradient where the Pliocene sediment wedge onlaps the slope (black circles in Fig. 9); (3) slope failures (evacuation zones in Fig. 9), which appear to be confined to the onlapping Pliocene wedge (see dashed line in Fig. 3), consistently occur 200 to 300 m downslope of the point of onlap where the wedge thickness exceeds 50 m.

DISCUSSION

Basin History, Preconditioning Factors, and Slope Instability

Although the slides observed in the SCB can be classified as open slope and predominantly translational in terms of failure initiation, our observations suggest that the failed masses mobilized into sediment flows as the material moved farther basinward (Varnes 1978, Hampton et al. 1996, Mulder and Cochonat 1996, Mulder and Alexander 2001). Initial failure occurred along stratigraphic contacts (failure planes), and the slide masses appear to have translated across the steep section of the lower slope (~7°) until reaching the flat basin floor. Although there are slide scarps present below the headwalls and within the failure zones (e.g., Figs. 3, 4), additional data are needed to determine if these scarps are related to earlier phases of retrogressive failure, or if they formed subsequent to the main slide event. Each of the distinguishable large slide deposits along the base of slope is emplaced above a seismic facies boundary inferred to represent the top of the Pliocene (Figs. 6, 7). The section of stacked landslide deposits along the base of slope appears to be interfingered with parallel-bedded fan deposits in the upper 300 m of basin fill (e.g., Fig. 7B), suggesting that failure of the uplifted Pliocene wedge occurred incrementally throughout the Quaternary.

As described previously, most of the present-day basin physiography of the SCB, including the platforms and slopes along SRCR anticlinorium, was established during the late Miocene and early Pliocene (Moore 1969, Field and Richmond 1980, Vedder 1987, Teng and Gorsline 1989). The Borderland was draped by Monterey-type diatomaceous sediment during the late Miocene, typically resulting in

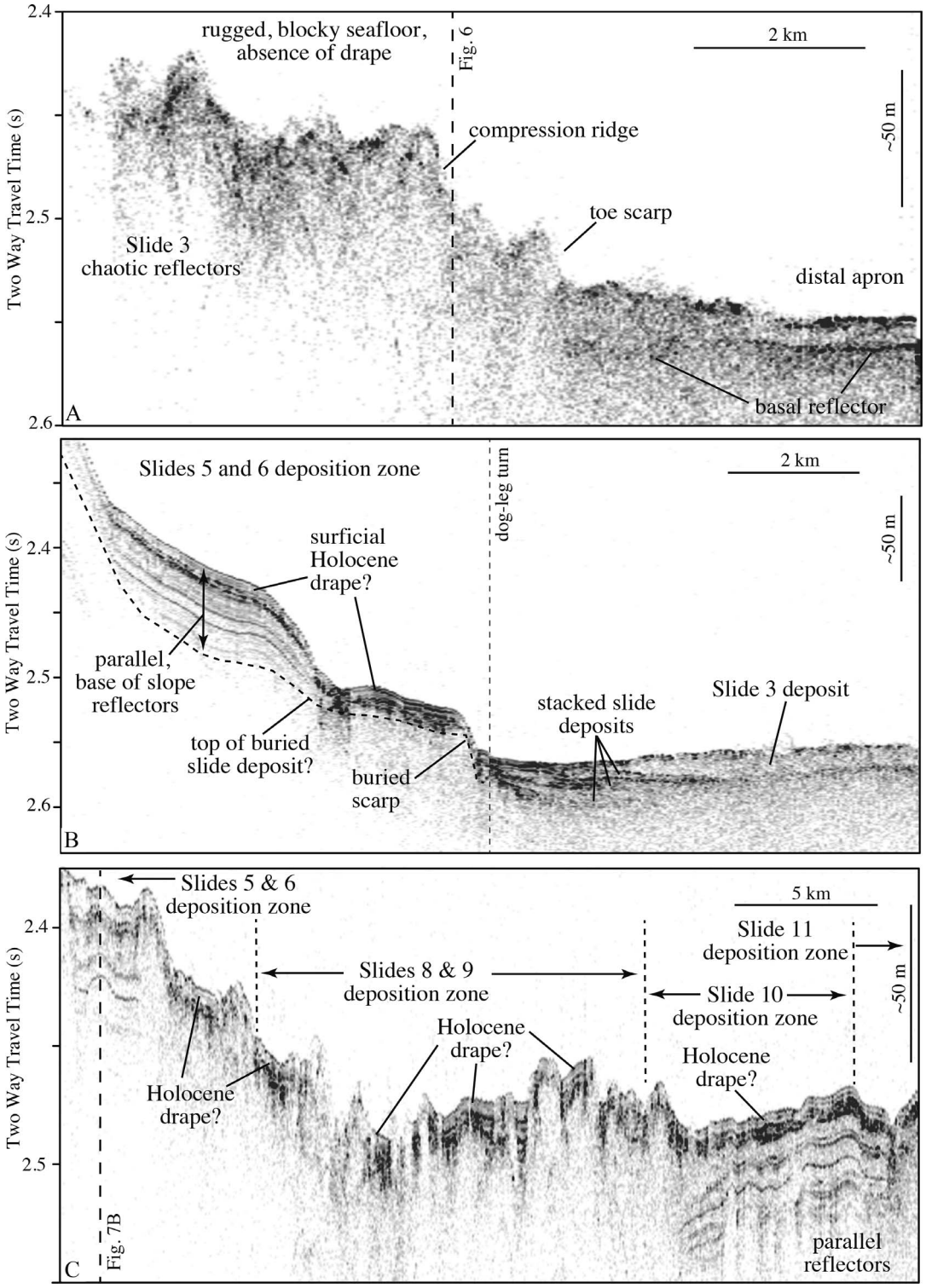

FIG. 8.—Subbottom Chirp profiles across **A)** slide 3, **B)** slides 3, 5 and 6, and **C)** slides 5-11. The thickness of sediment drape emplaced on top of slide deposits is used to estimate the relative ages of the slides; there is no resolvable drape on slide 3, suggesting it occurred relatively recently (i.e., mid- to late Holocene). Varying amounts of drape cover each of the other slides. See Figures 2 and 4 for profile locations.

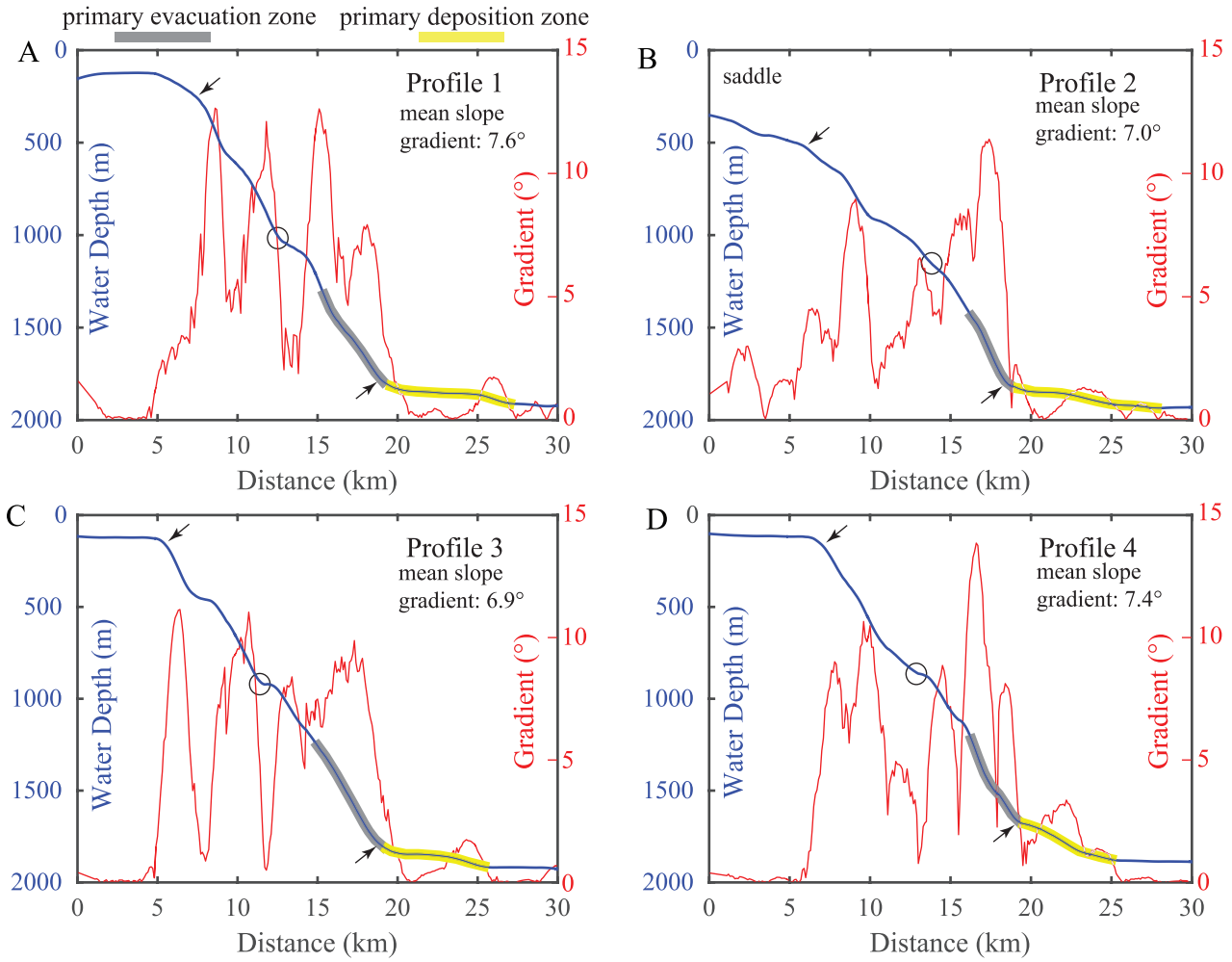

FIG. 9.—Bathymetric profiles extracted from the Coastal Relief Model (National Geophysical Data Center 2013) to examine the relationships between variations in steepness (gradient) and the Pliocene to present stratigraphic architecture. Profiles were smoothed using a 13 point Savitzky–Golay window. A decrease in profile gradient and the location of Pliocene stratal onlap (black circles) appear to be spatially correlated. Headwall scarps, located at the upslope limit of the evacuation zones (gray lines), are consistently located within the Pliocene wedge 3–5 km downslope of the position of onlap and where the wedge thickness exceeds 50 m. Black arrows bound the sections of the slopes used to compute the mean gradients. See Figure 2 for profile locations.

parallel-bedded stratigraphic horizons mantled across underlying surfaces (e.g., Figs. 5–7). Pliocene and Quaternary sedimentation was heavily influenced by basin morphology and gravity-driven processes that typically created basin stratigraphy that infilled topographic lows and onlapped surrounding basin margins. Thus, the reversal in stratal geometries between the Pliocene–Quaternary packages (i.e., onlap to the west–southwest) and the Miocene–older packages (parallel beds showing eastward thinning) records a shift in the regional tectonic regime (see schematic in Fig. 10; Moore 1969, Teng and Gorsline 1989, Schindler 2010) that is central to understanding the factors that preconditioned the eastern flank of the SRCR for failure. The post-Miocene onlap and basin infill imply that initiation of uplift along the SRCR anticlinorium was responsible for rotation of the Miocene section and creation of the SCB sediment sink. We propose that the stranded wedge of onlapping Pliocene strata along the east flank of the SRCR was originally emplaced in a nascent basin as horizontal layers on top of a late Miocene unconformity surface (see truncation surface in Fig. 5) and concurrent with the later stages of uplift along the anticlinorium (Fig. 10). As uplift continued into the early Pliocene, the onlapping wedge and the underlying Miocene sequences were tilted to roughly 7°, and the wedge became elevated above the basin floor by several hundred meters. Toward the late Pliocene and early Quaternary, uplift of the SRCR ended as the Borderland tectonic regime transitioned to strike-slip dominance (e.g., Bohannon and Geist 1998).

The inferred failure surface of each of the slides either coincides with or is very close to the Miocene–Pliocene boundary. Interestingly, there are no significant failures observed along the slope above the onlapping Pliocene wedge, where Miocene sediment is either exposed at the seafloor, or it is covered by a very thin veneer of Pleistocene and Holocene sediment (Nardin et al. 1979a, Field and Richmond 1980). Although sediment core data are needed to distinguish between lithological and geotechnical properties in the slide zones, patterns in the regional geology and dredge samples of the Miocene section of the

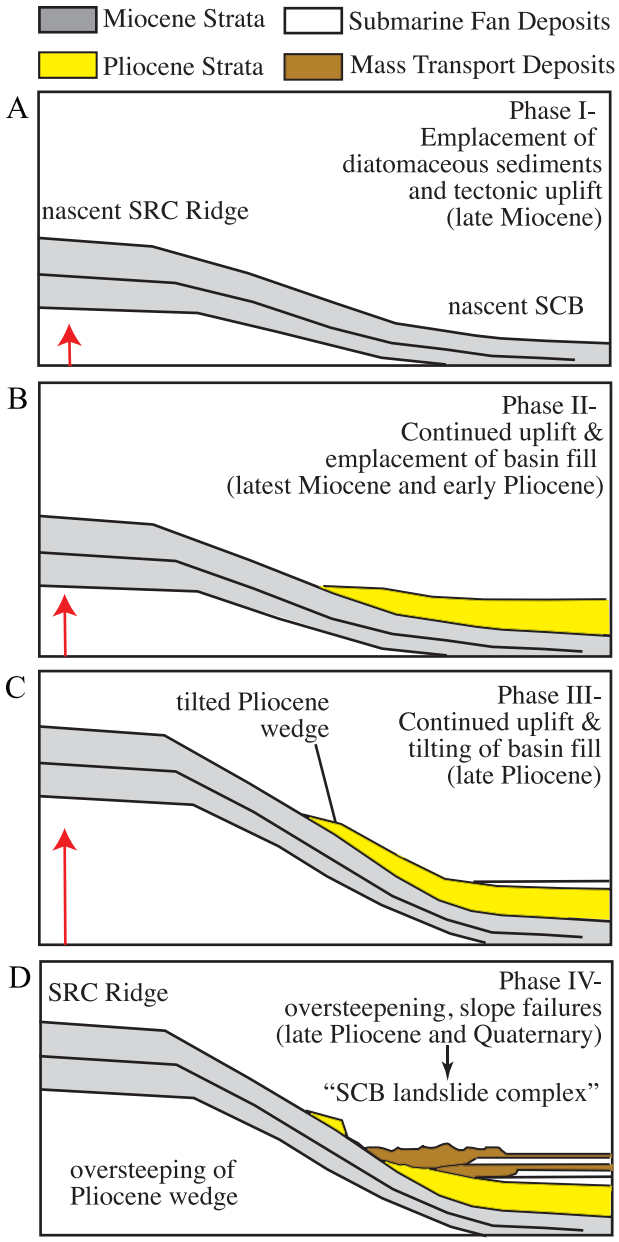

FIG. 10.—Proposed late Miocene to Quaternary development of the Santa Rosa–Cortes (SRC) Ridge, Santa Cruz Basin (SCB), and the "SCB landslide complex." **A)** Uplift began during the Miocene (gray layers) and continued into the Pliocene **B)**, leading to oversteepening of onlapping Pliocene strata (yellow layers) several hundred meters above the basin floor **C)**. This process preconditioned the stranded Pliocene strata along middle and lower slopes for failure and led the to the development of the SCB submarine landslide complex, as illustrated in part D. At present, mass transport deposits sourced from failures along the SRC Ridge (brown layers) are interfingered with submarine fan deposits (thin white layers) sourced primarily from nearby canyons. See "Discussion" section for details.

SRCR contain lithified diatomaceous siltstone, shale, and interbedded sandstone that are expected to be stable on slopes of 7° to 8°. In contrast, the Pliocene sediment emplaced in the Borderland basins generally contains a greater proportion of terrigenous material, including interbedded mudstone, sandstone, and minor amounts of conglomerate (Vedder et al. 1974). Based on the geometry of the Pliocene strata, and the observed character of the associated slide deposits, it is unlikely the Pliocene wedge was buried, diagenetically altered, and subsequently exhumed to its present position. We propose that uplift along the SRCR led to steepening of the Pliocene wedge and thus preconditioned it for failure and translational sliding along lithological contacts. Cyclic strength loss and application of downslope cyclic shear stresses during large earthquakes are likely triggers for episodic failure of the Pliocene stratigraphy.

Large landslides are expected to preferentially occur in accumulations of spatially continuous sedimentary masses (e.g., Hampton et al. 1996). Because the flank of the SRCR is a relatively smooth slope underlain by only minor amounts of stratigraphic heterogeneity, the uplifted Pliocene wedge defined a broad, uniformly dipping, and spatially continuous source of material prone to failure, meaning there were few morphological limitations on the size of failures (e.g., ten Brink et al. 2009). Furthermore, the upslope limit of the failures appears to be a function of Pliocene sediment thickness. In this case, the yield strength along the basal failure surface is exceeded where the onlapping Pliocene wedge exceeds a thickness of ~50 m. In contrast, the flank of the Santa Cruz–Catalina Ridge on the opposite side of the basin is characterized by a complicated regime of faults, folds, and ridges that restrict the spatial continuity of any particular slope and sedimentary deposit. We propose that failures on the eastern side of the basin would be smaller, and spatially confined to steep, localized slopes controlled by tectonic features, thus resulting in the generation of localized sediment flows and gully formation rather than large-scale slope failure.

Depositional Processes, Age Estimates, Triggering Mechanisms, and Tsunamigenic Potential

The morphology and internal character of slide deposits can provide insights into the dynamics and emplacement of failed sedimentary masses (e.g., Varnes 1978, Hampton et al. 1996, Mulder and Alexander 2001). Previous studies of subaqueous slides have separated such deposits into two classes based on the degree of compressional deformation and emplacement style (Frey-Martínez et al. 2006, Moernaut and De Batist 2011): Confined slides contain frontal thrust structures, including toe scarps, a significant degree of basal erosion, and rotated and/or folded blocks of coherent strata that have positive relief distinct from surrounding undisturbed basin sediments; emergent slides are less disruptive of the underlying strata and typically fan out between pre- and postfailure units. Deposits from slides 3, 8, and 9 appear to contain elements of both types. The hummocky, blocky, and wrinkled morphological expression of the slide deposits at the base of the slope (Figs. 3, 4), the evidence for intensely deformed internal reflectors in the proximal deposits (Figs. 6, 7A), and the acoustically transparent and/or chaotic components of the distal deposits all suggest that the slides represent a continuum of rheological behavior ranging from high-yield-strength and high-viscosity confined slides to the generation of low-yield-strength and low-viscosity emergent sediment flows (i.e., debris and turbidity flows) that extend across the basin floor. Deformed internal reflectors of the proximal deposits, evidence for thrusting and compressional deformations, and pervasive disruption and truncation of the underlying stratigraphy (e.g., Figs. 6, 7) suggest that the bulk of each slide is composed of relatively high-yield-strength, mobilized sediment. These masses translated 3 to 5 km down the lower slope

and appear to have impacted the basin floor with substantial force. The disruption at the base of the higher-strength component of the slides extends an additional 5 to 8 km basinward. The slide deposits then thin rapidly at a series of toe scarps and transition into parallel and subparallel beds that are interfingered with basin floor canyon/fan deposits. These gradational changes in deposit thickness, morphology, and internal character suggest that the slides experienced dynamic flow separation (e.g., Figs. 6, 7A), a process that was proposed by Nardin et al. (1979a) and has been observed in numerous other studies of subaqueous slide dynamics (Mulder and Alexander 2001, Mohrig and Marr 2003, Haflidason et al. 2004, Locat et al. 2009, Moernaut and De Batist 2011, Parsons et al. 2014, Brothers et al. 2016). Flow separation may result from variations in yield strengths within the failing mass. Material at its base is expected to be stronger than that at its surface due to compaction. If the slide experiences limited mixing as it is mobilized into a flow, then the weaker surface sediment will form into a more fluid (lower yield strength and viscosity) flow, and the deeper and stronger sediment will form a relatively less fluid flow. The initial acceleration, velocity, volume (mass), slide evolution (i.e., time between displacement of sections of the failing mass and time required to undergo flow transformation), and rheology are important parameters in the evaluation of the tsunamigenic potential for submarine landslides (Imran et al. 2001, Locat et al. 2004, Geist et al. 2009).

Two approaches can be used to provide rough age estimates for the large slides in the SCB. First, qualitative evaluation of the morphological expression of headwall scarps and associated debris aprons (greater angularity and roughness indicate relative recency) can be combined with stacking patterns and crosscutting relationships among deposits observed in the substrate; second, the thickness of sediment drape emplaced on failure surfaces and deposits can be used to estimate the relative ages of slides based on late Pleistocene and Holocene sediment accumulation rates. Several slides display a pronounced morphological expression despite burial beneath tens of meters of sediment drape. The draping layers most likely originate from a combination of hemipelagic and fine-grained suspended sediment (e.g., overbank deposits) sourced from debris and turbidity flows entering the basin (see Felsher 1971, Nardin et al. 1979a); their accumulation appears to have a rounding effect on sharper features while preserving the first-order morphology. We provide a qualitative ranking for the ages of the slides in Table 1, in which the youngest slides (3, 8, and 9) contain angular scarps and rugged, blocky debris aprons. Slide 3 is inferred to be the youngest in the basin (mid- to late Holocene) based on the absence of observable surficial drape on its debris apron (Fig. 8A).

Both hemipelagic accumulation and suspended sediment from nearby flows are potential sources for the accumulation of drape deposits. Sediment flows are known to reach the basin floor in the area proximal to the toe of the debris lobe (Figs. 2, 3) and are expected to generate plumes of fine-grained suspended sediment that settle onto features of positive relief proximal to the active Santa Cruz canyon/channel system. Hence, we do not expect the debris lobe of slide 3 to be an area of nondeposition during the Holocene. Although channel morphology observed in backscatter imagery (not shown herein; see data available at https://www.ngdc.noaa.gov/ships/okeanos_explorer/EX1101_mb.html) suggests emplacement of slide 3 may have preceded the most recent activity in the Santa Cruz channel/fan, an absolute age estimate for the slide cannot be determined without direct sampling. Slides 8 and 9 are inferred to be early Holocene or latest Pleistocene based on the thin layer (3–8 m) of drape observed above the debris apron and burial of the distal slide deposit. Slides 6 and 10 display slightly rounded headwall scarps and a greater drape (10–40 m) on the deposits and evacuation zones; deposits from both slides have visible morphological expression at the seabed. Both are inferred to be middle to late Pleistocene in age. Slide 7 is relatively small and may be roughly the same age as slide 6, based on the angularity of its headwall scarp. Deposits from slides 5 and 11 are roughly coincident stratigraphically (near the base of the Quaternary section), but the headwall and evacuation zones of slide 11 display significantly greater morphological disruption from gullying and other downslope sediment transport processes. Both are inferred to be early to mid-Pleistocene in age. Finally, slides 1 and 2, the oldest identifiable slides in the SCB (early Pleistocene?), have subtle expressions that are heavily modified by gully formation and sediment accumulation. In fact, slide 3 has evacuated postfailure sediment that accumulated below the headwalls of slides 1 and 2, suggesting the failure zones have experienced sediment recharge during the Quaternary.

Major thrust and strike-slip fault systems define the northern edge of the SCB and are responsible for uplift and deformation of the Channel Islands (Pinter and Sorlien 1991, Shaw and Suppe 1996). It is possible that large, but infrequent earthquakes along the Santa Cruz Island and Santa Rosa Island faults are capable of triggering slope failure in the Santa Cruz Basin (Chaytor et al. 2008, Seeber and Sorlien 2000). Although shaking from large-magnitude earthquakes is a likely triggering mechanism for the slides observed, the inferred ages of the individual slides suggest they occurred over a range of hundreds of thousands of years and have much lower recurrence than large earthquakes in the region. Despite the pervasive evidence for failure of the onlapping Pliocene strata, relatively thick sections of intact strata remain on east flank of the SRCR, particularly on either side of slide 3 (e.g., Figs. 3, 4, and 7B), suggesting that slides having similar characteristics could be generated in the future.

Comparisons to Other Submarine Landslides in Southern California

Prior to this study, the Goleta slide complex in the Santa Barbara Channel and the Palos Verdes debris avalanche off Los Angeles (Fig. 1) were the only major Holocene-aged submarine landslide complexes in southern California extensively studied using modern geophysical and geological techniques, and the only two determined to be have been tsunamigenic (Borrero et al. 2001, Bohannon and Gardner 2004, Fisher et al. 2005, Greene et al. 2006, Lee et al. 2009). Although previous studies documented the importance of mass wasting processes in the SCB, they did not resolve the scale or morphological details of the slide deposits and source regions. They also did not recognize or document relative differences in slide ages. The new high-resolution data and analyses presented herein have uncovered the largest submarine landslide complex in southern California, including what appear to be two or three of the largest late Pleistocene–Holocene-aged slides in southern California. The minimum area covered by slide evacuation zones and outer edges of the debris aprons is $\sim$160 km^2—this value does not include the area of basin floor covered by distal slide deposits (Table 1). Likewise, the minimum volume of sediment mobilized from the eastern flank of the SRCR is $\sim$13 km^3. We identified at least six individual failures that may have mobilized more than 1 km^3 of sediment; slides 8 and 9, which display only weak evidence for morphological separation, have a combined volume of $\sim$3.5 km^3, which is more than twice the size of the Goleta landslide complex in the Santa Barbara Basin and several times the size of the Palos Verdes debris avalanche.

Given the water depth, volume, evidence for dynamic flow separation, and observed runout, we propose that each of the slides described in this study could potentially have been tsunamigenic. Although the estimated runup along a 30-km-long stretch of the Santa Barbara coastline following the Goleta slide was estimated to be up to 10 m (Greene et al. 2006), the slide was roughly 5 km away from the zone of impact. In contrast, slides in the SCB are more than 60 km from the shoreline at Port Hueneme, and nearly 100 km away from the

Los Angeles area. The bathymetric and topographic complexity of the Borderland provides potential barriers between the mainland and the SCB, and tsunami height would be reduced due to attenuation. Thus, we expect the impact of such an event to be relatively minor. Due to their proximity (<10 km) to the SCB, slide-generated runup along the southern shorelines of the Channel Islands may be several meters high. Nevertheless, hydrodynamic modeling is needed to accurately evaluate the tsunami potential.

Given the extent of landslide features observed in the SCB, the remaining availability of perched, unstable Pliocene sediment along the steep flank of the SRCR, and the likelihood for seismic activity in southern California (Field et al. 2014), slope failure of some form in the future is likely. Due to the relatively narrow shelf and steep slopes along the continental margin, most terrigenous Quaternary sediment delivered to the shelf edge bypasses the slope and is deposited in fan/channel systems (Nardin et al. 1979b, Covault et al. 2007). Therefore, only a handful of places in the Borderland are expected to contain underconsolidated and unstable sedimentary deposits capable of generating large submarine landslides. We propose that other slides observed along steep flanks of basin margins throughout the Borderland, such as the smaller failures near the base of the slope adjacent to the Palos Verdes debris avalanche (Bohannon and Gardner 2004), also involved failure of uplifted and rotated Pliocene deposits. A systematic, high-resolution characterization of the underlying stratigraphic architecture throughout the Borderland may lead to fundamental advances in our understanding of the potential hazards to the southern California coastline. Finally, future studies involving sediment coring and age dating of slide deposits are needed, as well as numerical models to investigate slide dynamics and tsunami runup.

SUMMARY

As previously described, slope failure plays a fundamental role in the Pliocene and Quaternary evolution of the SCB. This study provides the first comprehensive characterization of the SCB submarine landslide complex using modern geophysical imaging techniques, including the first constraints on the full spatial extent of slide-related morphology, the character and dynamic evolution of slide masses, and the relative ages of individual failures. Failures appear to be confined to an onlapping wedge of Pliocene strata that was uplifted and tilted during the later stages of basin development. Slides appear to have occurred episodically throughout the Quaternary, and despite an absence of direct age control, the most recent failure appears to be mid- to late Holocene. Each of these observations suggests that the uplifted, oversteepened Pliocene section episodically fails, most likely during large earthquakes. Once mobilized, the failed material is transported several kilometers across a steep section of the lower slope and gains substantial momentum. The failed masses show evidence for dynamic separation into highly viscous and cohesive components that disturb underlying stratigraphy in areas most proximal to the source area, and low-viscosity, low-density sediment flows that blanket the underlying stratigraphy along the distal reaches of deposition. The volume of individual slides, cohesive character of the distal deposits, and inferred relatively high velocity during mobilization suggest that slides in the SCB were tsunamigenic. Because intact sections of Pliocene strata remain on the steep flank of the SRCR, the potential exists for future landslides that may impact the southern California coastline.

ACKNOWLEDGMENTS

This study was funded by the USGS Coastal and Marine Geology Program. We would like to thank Chuck Worley, Jackson Currie, Tom O'Brien, and Rob Wyland for technical assistance aboard the R/V *Robert Gordon Sproul*. Pete Dartnell, Brian Andrews, and Ray Sliter assisted in the compilation of marine geophysical data in the Santa Cruz Basin. We would also like to thank Bruce Applegate, Lana Graves, Emily Wei, and Neal Driscoll of the Scripps Institution of Oceanography for assisting at sea and contributing University of California student ship funds. We thank Homa Lee, Gary Greene, and an anonymous reviewer for providing helpful comments. Any use of trade, product, or firm names is for descriptive purposes only and does not imply endorsement by the US government.

REFERENCES

Astiz L, Shearer PM. 2000. Earthquake locations in the inner Continental Borderland, offshore southern California. *Bulletin of the Seismological Society of America* 90(2):425–449.

Atwater T, Stock J. 1998. Pacific–North America plate tectonics of the Neogene southwestern United States: An update. *International Geology Review* 40(5):375–402.

Barnes PW. 1970. Marine Geology and Oceanography of Santa Cruz Basin off Southern California: Report to U.S. Geological Survey, USC-GEOL 70-3, Menlo Park, California. 172 p.

Bohannon RG, Gardner JV. 2004. Submarine landslides of San Pedro Escarpment, southwest of Long Beach, California. *Marine Geology* 203(3):261–268.

Bohannon RG, Geist E. 1998. Upper crustal structure and Neogene tectonic development of the California continental borderland. *Geological Society of America Bulletin* 110(6):779–800.

Borrero JC, Dolan JF, Synolakis CE. 2001. Tsunamis within the eastern Santa Barbara Channel. *Geophysical Research Letters* 28(4):643–646.

Borrero JC, Legg MR, Synolakis CE. 2004. Tsunami sources in the southern California bight. *Geophysical Research Letters* 31(13):L13211. DOI:10.1029/2004GL0200478

Bouma AH, Kuenen PH, Shepard FP. 1962. *Sedimentology of Some Flysch Deposits: A Graphic Approach to Facies Interpretation*: Elsevier, Amsterdam. 168 p.

Brothers DS, Conrad JE, Maier KL, Paull CK, McGann M, Caress DW. 2015. The Palos Verdes Fault offshore Southern California: Late Pleistocene to present tectonic geomorphology, seascape evolution, and slip rate estimate based on AUV and ROV surveys. *Journal of Geophysical Research: Solid Earth* 120(7):4734–4758.

Brothers DS, Haeussler PJ, Liberty L, Finlayson DP, Geist E, Labay K, Byerly M. 2016. A submarine landslide source for the devastating 1964 Chenega tsunami, southern Alaska. *Earth and Planetary Science Letters* 438(15):112–121.

Chaytor JD. 2006. Diffuse deformation patterns along the North American plate boundary zone, offshore western United States [PhD thesis]: Oregon State University, Corvallis, Oregon, 299 p.

Chaytor JD, Goldfinger C, Meiner MA, Huftile GJ, Romsos CG, Legg MR. 2008. Measuring vertical tectonic motion at the intersection of the Santa Cruz–Catalina Ridge and Northern Channel Islands platform, California Continental Borderland, using submerged paleoshorelines. *Geological Society of America Bulletin* 120(7–8):1053–1071.

Conrad JE, Brothers DS, Maier KL, Ryan HF, Dartnell P, Sliter RW. 2018. Right-lateral fault motion along the slope-basin transition, Gulf of Santa Catalina, southern California. *In* Marsaglia KM, Schwalbach JR, Behl RJ (Editors). *From the Mountains to the Abyss: The California Borderland as an Archive of Southern California Geologic Evolution*, Special Publication 110: SEPM (Society for Sedimentary Geology), Tulsa, Oklahoma. DOI:10.2110/sepmsp.110.XX

Covault JA, Normark WR, Romans BW, Graham SA. 2007. Highstand fans in the California borderland: The overlooked deep-water depositional systems. *Geology* 35(9):783–786.

Crouch JK, Suppe J. 1993. Late Cenozoic tectonic evolution of the Los Angeles Basin and inner California Borderland: A model for core complex-like crustal extension. *Geological Society of America Bulletin* 105(11):1415–1434.

Dartnell P, Driscoll NW, Brothers DS, Conrad JE, Kluesner JW, Kent GM. 2015. *Colored Shaded-Relief Bathymetry, Acoustic Backscatter, and Selected Perspective Views of the Inner Continental Borderland, Southern California*:

U.S. Geological Survey, Scientific Investigations Map 3324, 3 plates. https://pubs.usgs.gov/sim3324

Felsher M. 1971. Physical sedimentary and bathymetry, Santa Cruz submarine canyon complex, Contintenal Borderland, California [PhD thesis]: University of Texas at Austin, 331 p.

Field EH, Arrowsmith RJ, Biasi GP, Bird P, Dawson TE, Felzer KR, Jackson DD, Johnson KM, Jordan TH, Madden C. 2014. Uniform California Earthquake Rupture Forecast, version 3 (UCERF3)—The time-independent model. *Bulletin of the Seismological Society of America* 104(3):1122–1180.

Field ME, Edwards BD. 1980. Slopes of the southern California continental borderland: A regime of mass transport. *In* Field ME, Bouma AH, Colbourn IP, Douglas RG, Ingle VC (Editors). Pacific Coast Paleogeography Symposium 4: Society of Economic Paleontologists and Mineralogists, Pacific Section, Bakersfield, California. p. 169–184.

Field ME, Richmond WC. 1980. Sedimentary and structural patterns on the northern Santa Rosa–Cortes Ridge, southern California. *Marine Geology* 34(1):79–98.

Fisher MA, Normark WR, Greene HG, Lee HJ, Sliter RW. 2005. Geology and tsunamigenic potential of submarine landslides in Santa Barbara Channel, Southern California. *Marine Geology* 224(1):1–22.

Fisher MA, Normark WR, Langenheim VE, Calvert AJ, Sliter R. 2004. The offshore Palos Verdes Fault Zone near San Pedro, Southern California. *Bulletin of the Seismological Society of America* 94(2):506–530.

Frey-Martínez J, Cartwright J, James D. 2006. Frontally confined versus frontally emergent submarine landslides: A 3D seismic characterisation. *Marine and Petroleum Geology* 23(5):585–604.

Geist EL, Lynett PJ, Chaytor JD. 2009. Hydrodynamic modeling of tsunamis from the Currituck landslide. *Marine Geology* 264(1):41–52.

Gorsline DS, Barnes PW. 1972. Carbonate variations as climatic indicators in contemporary California flysch basins. *In* 24th International Geological Congress, Section 6, Montreal, p. 270–277.

Greene HG, Clarke SH, Field ME, Linker FI, Wagner HC. 1975. Preliminary Report on the Environmental Geology of Selected Areas of the Southern California Continental Borderland: U.S. Geological Survey, Open-File Report 75-596, 70 p.

Greene HG, Murai LY, Watts P, Maher NA, Fisher MA, Paull CE, Eichhubl P. 2006. Submarine landslides in the Santa Barbara Channel as potential tsunami sources. *Natural Hazards and Earth System Science* 6(1):63–88.

Haflidason H, Sejrup HP, Nygård A, Mienert J, Bryn P, Lien R, Forsberg CF, Berg K, Masson D. 2004. The Storegga Slide: Architecture, geometry and slide development. *Marine Geology* 213(1):201–234.

Hampton MA, Lee HJ, Locat J. 1996. Submarine landslides. *Reviews of Geophysics* 34(1):33–59.

Imran J, Parker G, Locat J, Lee H. 2001. 1D numerical model of muddy subaqueous and subaerial debris flows. *Journal of Hydraulic Engineering* 127(11):959–968.

Junger A. 1976. Offshore structure between Santa Cruz and Santa Rosa islands. *In* Howell DG (Editor). *Aspects of the Geologic History of the California Borderland*, Miscellaneous Publication 24: American Association of Petroleum Geologists, Pacific Section, p. 418–426.

Kamerling MJ, Luyendyk BP. 1985. Paleomagnetism and Neogene tectonics of the northern Channel Islands, California. *Journal of Geophysical Research: Solid Earth* 90(B14):12485–12502.

Lee HJ, Greene HG, Edwards BD, Fisher MA, Normark WR. 2009. Submarine landslides of the Southern California Borderland. *In* Lee HJ, Normark WR (Editors). *Earth Science in the Urban Ocean: The Southern California Continental Borderland*, Special Paper 454: Geological Society of America, Boulder, Colorado. p. 251–269.

Legg MR. 1991. Developments in understanding the evolution of the California Continental Borderland. *In* Osborne RH (Editor). *From Shoreline to Abyss: Contributions to Marine Geology in Honor of Francis Parker Shepard*, Special Publication 46: SEPM (Society for Sedimentary Geology), Tulsa, Oklahoma. p. 291–312.

Legg MR, Goldfinger C, Kamerling M, Chaytor J, Einstein D. 2007. Morphology, structure and evolution of California Continental Borderland restraining bends. *In* Cunningham WD, Mann P (Editors). *Tectonics of Strike-Slip Restraining and Releasing Bends*, Special Publication 290: Geological Society, London. p. 143–168.

Legg MR, Kohler MD, Shintaku N, Weeraratne DS. 2015. High-resolution mapping of two large-scale transpressional fault zones in the California Continental Borderland: Santa Cruz–Catalina Ridge and Ferrelo faults. *Journal of Geophysical Research: Earth Surface* 120(5):915–942.

Lindvall SC, Rockwell TK. 1995. Holocene activity of the Rose Canyon Fault Zone in San Diego, California. *Journal of Geophysical Research: Solid Earth* 100(B12):24121–24132.

Locat J, Lee H, Locat P, Imran J. 2004. Numerical analysis of the mobility of the Palos Verdes debris avalanche, California, and its implication for the generation of tsunamis. *Marine Geology* 203(3):269–280.

Locat J, Lee H, ten Brink US, Twichell D, Geist E, Sansoucy M. 2009. Geomorphology, stability and mobility of the Currituck slide. *Marine Geology* 264(1):28–40.

Mitchum RM, Vail P, Thompson S. 1977. Seismic stratigraphy and global changes of sea level; Part 2. The depositional sequence as a basic unit for stratigraphic anlysis. *In* Payton CE (Editor). *Seismic Stratigraphy; Applications to Hydrocarbon Exploration*, Memoir 26: American Association of Petroleum Geologists, Tulsa, Oklahoma. p. 53–62.

Moernaut J, De Batist M. 2011. Frontal emplacement and mobility of sublacustrine landslides: Results from morphometric and seismostratigraphic analysis. *Marine Geology* 285(1):29–45.

Mohrig D, Marr JG. 2003. Constraining the efficiency of turbidity current generation from submarine debris flows and slides using laboratory experiments. *Marine and Petroleum Geology* 20(6–8):883–899.

Moore DG. 1969. *Reflection Profiling Studies of the California Continental Borderland: Structure and Quaternary Turbidite Basins*, Special Paper 107: Geological Society of America, Boulder, Colorado. 142 p.

Mulder T, Alexander J. 2001. The physical character of subaqueous sedimentary density flows and their deposits. *Sedimentology* 48(2):269–299.

Mulder T, Cochonat P. 1996. Classification of offshore mass movements. *Journal of Sedimentary Research* 66(1):43–57.

Nardin TR, Edwards BD, Gorsline DS. 1979a. Santa Cruz Basin, California Borderland: Dominance of slope processes in basin sedimentation. *In* Doyle LJ, Pilkey OH (Editors). *Geology of Continental Slopes*, Special Publication 27: Society of Economic Paleontologists and Mineralogists, Tulsa, Oklahoma. p. 209–221.

Nardin TR, Hein FJ, Gorsline DS, Edwards BD. 1979b. A review of mass movement processes, sediment and acoustic characteristics, and contrasts in slope and base-of-slope systems versus canyon-fan-basin floor systems. *In* Doyle LJ, Pilkey OH (Editors). *Geology of Continental Slopes*, Special Publication 27: Society of Economic Paleontologists and Mineralogists, Tulsa, Oklahoma. p. 61–73.

National Geophysical Data Center. 2013. US Coastal Relief Model–Southern California, Vers. 2: National Geophysical Data Center, NOAA, Boulder, Colorado. https://www.ngdc.noaa.gov. Accessed February 2016.

Nicholson C, Sorlien CC, Atwater T, Crowell JC, Luyendyk BP. 1994. Microplate capture, rotation of the western Transverse Ranges, and initiation of the San Andreas Transform as a low-angle fault system. *Geology* 22(6):491–495.

Parsons T, Geist EL, Ryan HF, Lee HJ, Haeussler PJ, Lynett P, Hart PE, Sliter RW, Roland E. 2014. Source and progression of a submarine landslide and tsunami: The 1964 Great Alaska earthquake at Valdez. *Journal of Geophysical Research: Solid Earth* 119(11):8502–8516.

Pinter N, Sorlien CC. 1991. Evidence for latest Pleistocene to Holocene movement on the Santa Cruz Island fault, California. *Geology* 19:909–912.

Ryan HF, Conrad JE, Paull CK, McGann M. 2012. Slip rate on the San Diego Trough Fault Zone, Inner California Borderland, and the 1986 Oceanside earthquake swarm revisited. *Bulletin of the Seismological Society of America* 102(6):2300–2312.

Ryan HF, Legg MR, Conrad JE, Sliter RW. 2009. Recent faulting in the Gulf of Santa Catalina: San Diego to Dana Point. *In* Lee HJ, Normark WR (Editors). *Earth Science in the Urban Ocean: The Southern California Continental Borderland*, Special Paper 454: Geological Society of America, Boulder, Colorado. p. 291–315.

Ryan KJ, Geist EL, Barall M, Oglesby DD. 2015. Dynamic models of an earthquake and tsunami offshore Ventura, California. *Geophysical Research Letters* 42(16):6599–6606.

Schindler CS. 2010. 3D fault geometry and basin evolution in the northern Continental Borderland offshore Southern California [MS thesis]: California State University, Bakersfield. 42 p.

Schwalbach JR, Edwards BD, Gorsline DS. 1996. Contemporary channel–levee systems in active borderland basin plains, California Continental Borderland. *Sedimentary Geology* 104(1):53–72.

Schwalbach JR, Gorsline DS. 1985. Holocene sediment budgets for the basins of the California continental borderland. *Journal of Sedimentary Research* 55(6):829–842.

Seeber L, Sorlien CC. 2000. Listric thrusts in the western Transverse Ranges, California. *Geological Society of America Bulletin* 112(7):1067–1079.

Shaw JH, Suppe J. 1996. Earthquake hazards of active blind-thrust faults under the central Los Angeles Basin, California. *Journal of Geophysical Research: Solid Earth* 101(B4):8623–8642.

Shepard FP, Emery KO. 1941. *Submarine Topography off the California Coast: Canyons and Tectonic Interpretations*, Special Paper 31: Geological Society of America, Boulder, Colorado. 171 p.

Sliter RW, Conrad JR, Brothers DS, Balster-Gee AF. 2017. Minisparker and Chirp Seismic-Reflection Data of Field Activity 2014-645-FA: Offshore Santa Barbara, Southern California from 2014-11-12 to 2014-11-25: U.S. Geological Survey, data release. DOI:10.5066/F7CV4FW6

ten Brink US, Barkan R, Andrews BD, Chaytor JD. 2009. Size distributions and failure initiation of submarine and subaerial landslides. *Earth and Planetary Science Letters* 287(1–2):31–42.

ten Brink US, Zhang J, Brocher TM, Okaya DM, Klitgord KD, Fuis GS. 2000. Geophysical evidence for the evolution of the California Inner Continental Borderland as a metamorphic core complex. *Journal of Geophysical Research: Solid Earth* 105(B3):5835–5857.

Teng LS, Gorsline DS. 1989. Late Cenozoic sedimentation in California continental borderland basins as revealed by seismic facies analysis. *Geological Society of America Bulletin* 101(1):27–41.

Varnes DJ. 1978. Slope movement types and processes. *In* Schuster RL, Krizek RJ (Editors). *Landslides—Analysis and Control*, Special Report 176: National Research Council, Transportation Research Board, Washington, DC. p. 11–33.

Vedder JG. 1987. Regional geology and petroleum potential of the Southern California Borderland. *In* Gantz A (Editor). *Geology and Resource Potential of the Continental Margin of Western North Amerca and Adjacent Ocean Basins, Beaufort Sea to Baja California*: Circum-Pacific Council for Energy and Mineral Resources, Houston, Texas. p. 403–447.

Vedder JG, Beyer LA, Junger A, Moore GW, Roberts AE, Taylor JC, Wagner HC. 1974. *Preliminary Report on the Geology of the Continental Borderland of Southern California*: U.S. Geological Survey, Miscellaneous Field Studies Map 624, Reston, Virginia. 34 p., 9 plates.

Vedder JG, Howell DG. 1980. Topographic evolution of the southern California borderland during late Cenozoic time. *In* Power DM (Editor). *The California Islands: Proceedings of a Multidisciplinary Symposium*: Santa Barbara Museum of Natural History, Santa Barbara, California. p. 7–31.